



University
of Glasgow

Hein, A.S. and Hulton, N.R.J. and Dunai, T.J. and Schnabel, C. and Kaplan, M.R. and Naylor, M. and Xu, S. (2009) *Middle pleistocene glaciation in Patagonia dated by cosmogenic-nuclide measurements on outwash gravels*. *Earth and Planetary Science Letters*, 286 (1-2). pp. 184-197. ISSN 0012-821X

<http://eprints.gla.ac.uk/8326/>

Deposited on: 17 November 2009

1 **Middle Pleistocene glaciation in Patagonia dated by cosmogenic-**
2 **nuclide measurements on outwash gravels**

3
4 Hein, Andrew S.^a – *corresponding author**

5 Hulton, Nicholas R.J.^a

6 Dunai, Tibor J.^a

7 Schnabel, Christoph^b

8 Kaplan, Michael R.^c

9 Naylor, Mark^a

10 Xu, Sheng^b

11

12 ^a University of Edinburgh

13 School of Geosciences

14 Geography Building

15 Drummond Street, Edinburgh, EH8 9XP

16 United Kingdom

17 *a.s.hein@sms.ed.ac.uk

18 +44 (0) 131 650 2661

19 fax: +44 (0) 131 650 2524

20 Nick.Hulton@ed.ac.uk

21 Tibor.Dunai@ed.ac.uk

22

23 ^b Scottish Universities Environmental Research Centre

24 Scottish Enterprise Technology Park

25 East Kilbride, G75 0QF

26 United Kingdom

27 C.Schnabel@suerc.gla.ac.uk

28 s.xu@suerc.gla.ac.uk

29

30 ^c Lamont-Doherty Earth Observatory

31 Columbia University

32 Geochemistry

33 61 Route 9W - PO Box 1000

34 Palisades, NY, 10964-8000
35 United States of America
36 mkaplan@ldeo.columbia.edu

37

38 **Abstract**

39 The well-preserved glacial record in Argentine Patagonia offers a ~1 Ma archive of
40 terrestrial climate extremes in southern South America. These glacial deposits remain
41 largely undated beyond the range of radiocarbon dating at ca. 40 ka. Dating old
42 glacial deposits (> several 10^5 a) by cosmogenic surface exposure methods is
43 problematic because of the uncertainty in moraine degradation and boulder erosion
44 rates. Here, we show that cobbles on outwash terraces can reliably date ‘old’ glacial
45 deposits in the Lago Pueyrredón valley, 47.5° S, Argentina. Favorable environmental
46 conditions (e.g., aridity and strong winds) have enabled continuous surface exposure
47 of cobbles and preservation of outwash terraces. The data demonstrate that nuclide
48 inheritance is negligible and we therefore use the oldest surface cobbles to date the
49 deposit. ^{10}Be concentrations in outwash cobbles reveal a major glacial advance at ca.
50 260 ka, concurrent with Marine Isotope Stage 8 (MIS 8) and dust peaks in Antarctic
51 ice cores. A ^{10}Be concentration depth-profile in the outwash terrace supports the age
52 and suggests a low terrace erosion rate of ca. 0.5 mm ka^{-1} . We compare these data to
53 exposure ages obtained from associated moraines and find that surface boulders
54 under-estimate the age of the glaciation by ~100 ka; thus the oldest boulders in this
55 area do not date closely moraine deposition. The ^{10}Be concentration in moraine
56 cobbles help to constrain moraine degradation rates. These data together with
57 constraints from measured $^{26}\text{Al}/^{10}\text{Be}$ ratios suggest that all moraine boulders were
58 likely exhumed after original deposition. We determine the local Last Glacial
59 Maximum (LGM) occurred at ~27 – 25 ka, consistent with the maximum LGM in
60 other parts of Patagonia.

61

62 *Keywords:* Cosmogenic nuclide surface exposure dating; Marine Isotope Stage 8;
63 Glacial chronology; Southern South America; Beryllium-10; Last Glacial Maximum.

64

65

66 **1. INTRODUCTION**

67

68 The aim of this research is to establish a more reliable method of dating pre-Last
69 Glacial Maximum (LGM) ice limits using cosmogenic surface exposure dating
70 methods on glacial outwash terrace material as opposed to moraine boulders.
71 Specifically, this approach is used to date the well-preserved sequence of Quaternary
72 ice limits in Argentine Patagonia. These limits are well documented (e.g., Caldenius,
73 1932; Clapperton, 1993; Flint and Fidalgo, 1964; Mercer, 1976; Rabassa and
74 Clapperton, 1990; Singer et al., 2004) but have proved difficult to date thus far. Our
75 approach is to avoid the problems that inadvertently arise from dating boulders that
76 have been exhumed as a moraine degrades. We achieve this by sampling fluvial
77 rounded cobbles from stable outwash terrace surfaces that are stratigraphically
78 associated with the moraines. Applicability of the method is dependent on three
79 principal factors: First, linking outwash abandonment to a specific glacial event;
80 second, on there being low nuclide inheritance in outwash sediment; and third, that
81 there is no post-depositional burial, mixing or removal of the terrace sediment. We
82 argue that these favorable conditions are met in parts of Argentine Patagonia and may
83 occur in other arid and aeolian active environments elsewhere. In this paper, we
84 compare ^{10}Be exposure ages obtained from (1) moraine boulders with (2) moraine
85 cobbles and (3) outwash terrace cobbles of the same glacial event in the Lago
86 Pueyrredón valley, 47.5° S, Argentina. The palaeoclimatic significance of the new
87 chronology developed in this study will be addressed in future publications.

88

89 **1.1 Patagonian glacial history and the age gap**

90

91 Well-dated moraines older than the LGM are sparse in Patagonia reflecting a lack of
92 dateable material and the limit of radiocarbon dating beyond ~40 ka. Most outlet
93 valleys in arid Argentine Patagonia contain four to five groups of moraines and
94 associated outwash terraces (Caldenius, 1932; Clapperton, 1993; Kaplan et al., 2009).
95 The deposits range from the innermost LGM (~25 ka) deposits to the outermost
96 ‘Greatest Patagonian Glaciation’ deposits dated at ~1.1 Ma (Meglioli, 1992; Mercer,
97 1976; Rabassa and Clapperton, 1990; Rabassa et al., 2000; Singer et al., 2004; Ton-
98 That et al., 1999). In many cases, these end members often provide the only age
99 framework for intermediate deposits (i.e. between LGM time and ~1.1 Ma).
100 Recently, Kaplan et al. (2005) demonstrated the potential of cosmogenic surface
101 exposure methods to fill these gaps when they identified a glacial advance around 140
102 – 150 ka (MIS 6) and at least one prior to 200 ka at Lago Buenos Aires (LBA), 46.5°
103 S, Argentina. Despite good moraine preservation and low boulder erosion rates (~1.4
104 mm ka⁻¹), the wide scatter in boulder exposure ages made interpretation of the age of
105 older moraines challenging.

106

107 **1.2 Exposure dating of old moraines**

108

109 Boulders on old moraines (i.e., older than several 10⁵ a) frequently yield wide scatter
110 in exposure ages that is commonly attributed to boulder erosion rate uncertainty and
111 exhumation (e.g., Benson et al., 2004; Briner et al., 2005; Kaplan et al., 2007; Kaplan
112 et al., 2005; Owen et al., 2006; Phillips et al., 1990; Schäfer et al., 2008; Shanahan
113 and Zreda, 2000). Poorly constrained (or non steady-state) boulder erosion rates are
114 known to affect significantly the accuracy of older exposure ages, even with relatively
115 low rates of 1 mm ka⁻¹ (Gillespie and Bierman, 1995). Moraine degradation leads to

116 erroneously young boulder exposure ages (Hallet and Putkonen, 1994; Phillips et al.,
117 1990; Putkonen and Swanson, 2003; Zreda et al., 1994) and therefore the oldest
118 boulder can be used to date the deposit (cf. Zreda and Phillips, 1995). However, the
119 rate of degradation is site-specific and is rarely quantifiable. Without additional
120 constraints, the amount of moraine degradation and its effect on boulder exposure
121 ages remains difficult to assess and is not routinely considered. Recent model
122 findings suggest degradation may be ubiquitous and high (Putkonen et al., 2008;
123 Putkonen and O'Neal, 2006); thus even the oldest boulder ages may not date closely
124 moraine deposition. The increasing uncertainty on exhumation and erosion rates with
125 increasing moraine ages often limits the results to minimum limiting ages.

126

127 **1.3 Exposure dating of outwash terraces**

128

129 Glacial outwash terraces can often be directly linked to moraines that mark former ice
130 limits. They are frequently better preserved than moraines owing to their low-
131 gradient surfaces which are less prone to degradation. The surfaces may contain
132 fluvial rounded cobbles and original surface channel morphology that, providing the
133 terrace has not been reactivated post-depositionally, indicate minimal clast erosion or
134 exhumation since deposition. This suggests outwash terraces may be feasible for
135 exposure dating. However, small clasts on flat surfaces are more prone to burial (e.g.,
136 seasonal snow cover, soil, loess) and mixing (e.g., cryo- or bio-turbation, up-freezing,
137 overturning) than large moraine boulders, which together with potential aeolian
138 inflation or deflation of the terrace surface, can complicate the exposure history
139 (Gosse and Phillips, 2001).

140

141 Fluvial terraces associated with glacial events have been dated in previous studies
142 (e.g., Brocard et al., 2003; Chadwick et al., 1997; Hancock et al., 1999; Phillips et al.,
143 1997; Repka et al., 1997; Schildgen et al., 2002). Surface clasts may contain inherited
144 nuclides obtained prior to mobilization and during clast transport to the site of final
145 deposition. Methods have been developed to quantify the average nuclide inheritance
146 in a fluvial deposit (e.g., Anderson et al., 1996; Hancock et al., 1999; Repka et al.,
147 1997), but nuclide inheritance in individual clasts can vary significantly around this
148 mean (e.g., Hancock et al., 1999). Zentmire et al. (1999) measured ^{10}Be
149 concentrations in cobbles of modern day glacial outwash. These samples contained
150 negligible inherited nuclides which they attribute to both sub-glacial erosion and
151 shielding by the overriding glacier prior to deposition (Gosse and Phillips, 2001). If
152 both nuclide inheritance and clast mixing can be shown to be negligible, and $^{26}\text{Al}/^{10}\text{Be}$
153 ratios indicate no prolonged burial, then individual surface clasts from outwash
154 terraces could be suitable targets for dating old glacial events in regions where
155 boulder exhumation and erosion is an issue. With this in mind, we targeted a well-
156 preserved moraine and outwash sequence in Patagonia.

157

158 **2. LAGO PUEYRREDÓN VALLEY, 47.5° S, ARGENTINA**

159

160 The Lago Pueyrredón (LP) valley (Figure 1) was a major outlet of former Patagonian
161 ice sheets and the glacial record is exceptionally well-preserved (Figure 2). It is
162 located in close proximity to the dated long-term glacial record at Lago Buenos Aires
163 (LBA).

164

165 **2.1 Geology**

166

167 The LP valley is a west – east trending glacial depression separating the Meseta del
168 Lago Buenos Aires to the north and the Mesetas Belgrano and Olnie to the south
169 (Figure 2). The nearest granitic rocks are within the San Lorenzo Plutonic Complex,
170 about 80 km from the innermost moraines (Suárez and De La Cruz, 2001). The
171 nearest sources for quartz cobbles are veins in the Eastern Andes Metamorphic
172 Complex located 65 km west of the innermost moraines; thus clast transport distances
173 of the sampled lithologies are large.

174

175 Based on the pioneering work of Caldenius (1932), four major glacial units are
176 distinguished over a range of 40 km with the outermost deposits situated more than
177 350 meters higher than the innermost (Figure 2). Each unit is separated by
178 escarpments of up to 100 meters. This over-deepened valley shares a peculiarity in
179 drainage common throughout Patagonia; lakes and rivers on the eastern mountain
180 front drain to the Pacific Ocean, except during glacial times when the continuous N –
181 S oriented ice sheet forced drainage eastward to the Atlantic Ocean (Figure 1a). This
182 unique hydrologic condition is partly responsible for the exceptional preservation of
183 the deposits. Pre-LGM outwash terraces are also well-preserved because the trend in
184 ice extent has in general decreased over time (Kaplan et al., 2009). During glacial
185 maxima, melt-water discharged directly onto broad outwash plains until ice began to
186 retreat and pro-glacial lakes formed, dammed by terminal moraines. This caused
187 rivers to incise in response to the decreased sediment load (cf. Chorley et al., 1984),
188 thereby abandoning outwash terraces. Pro-glacial lakes are evident by the preserved
189 shorelines below the Hatcher and Río Blanco moraines (Figure 2), these eventually
190 drained westward when the Río Baker depression became ice free (Figure 1a; Mercer,

191 1976). We infer that outwash terraces stabilized shortly after glacial maximum
192 conditions.

193

194 **2.2 Climate**

195

196 The current climate in the study area is semi-arid with precipitation levels of 200 mm
197 a⁻¹ and strong and persistent winds¹. Annual snow cover is thin and short-lived (Local
198 land owners, personal communication) and models predict increased aridity during
199 glacial times (Hulton et al., 2002). Also, strong winds quickly removed ash deposited
200 by the 1991 eruption of Volcán Hudson in Chile (Inbar et al., 1995) and an increase in
201 the vigor of atmospheric circulation during glacial times (Petit et al., 1999) would
202 likely lead to higher wind velocities. Wind has observably been a dominant agent of
203 erosion with boulders commonly exhibiting ventifacts and flutings (Figure 3a).
204 Cobbles and pebbles on the Hatcher outwash terrace often exhibit rock varnish on
205 ventifacts (Figure 3b) suggesting aeolian erosion was not recent. We propose that
206 aeolian erosion was episodic in nature, occurring during glacial maxima when
207 outwash plains were active, devoid of vegetation and debris was available for
208 entrainment by wind (cf. Sugden et al., 2009). Therefore, we assume that post-
209 depositional shielding by annual snow cover, loess or other deposits is limited today
210 and during glacial times, even on flat outwash terraces.

211

212 **2.3 Existing glacial chronology**

213

¹ NCEP/NCAR reanalysis; www.cdc.noaa.gov/ncep_reanalysis/

214 The glacial chronology at Lago Pueyrredón previously was poorly developed. There
215 is no direct chronology for the deposits at Lago Pueyrredón. The only dates come
216 from three sources: First, Sylwan et al. (1991) measured magnetic polarity in glacial
217 sediments and found that part of the outermost mapped Caracoles unit was deposited
218 during the reversed Matuyama chron at more than 780 ka (Singer and Pringle, 1996);
219 second, Mercer (1976; 1982) dated peat in the former melt-water drainage near the
220 entrance to the Cañadón de Caracoles at ~ 11.8 ^{14}C ka (Figure 2), providing a
221 minimum age for the Río Blanco moraines (Wenzens, 2005); third, Wenzens (2005)
222 dated a mollusc shell from a lake deposit at the foot of the Cañadón de Caracoles
223 escarpment, inside the limit of the Hatcher moraines. The date of ~ 17.2 ^{14}C ka led
224 Wenzens (2005) to conclude that the Hatcher moraines were deposited during the
225 LGM as proposed by Caldenius (1932), and the Río Blanco moraines must therefore
226 be late glacial in age. However, the lack of a firm chronology makes correlation to
227 deposits in nearby valleys tentative and subject to debate (Kaplan et al., 2006;
228 Wenzens, 2006). Additional age limits were estimated (initially, before results were
229 obtained) based on correlation of Caldenius' (1932) mapping with deposits dated at
230 LBA (Figure 1b). Four major moraine groups are identified in both valleys. At LBA,
231 cosmogenic dating of the Fenix and Moreno I-II moraines indicated they are LGM
232 (~ 16 - 23 ka; Douglass et al., 2006; Kaplan et al., 2004), and MIS 6 in age (~ 140 - 150
233 ka; Kaplan et al., 2005). Steadily older glacial events are represented through the mid
234 Quaternary (~ 1.1 Ma) based on limiting $^{40}\text{Ar}/^{39}\text{Ar}$ ages (Singer et al., 2004).

235

236 **3. APPROACH AND METHODOLOGY**

237

238 To assess whether old glacial deposits can be dated more reliably using outwash
239 terrace cobbles as opposed to moraine boulders, we compare ^{10}Be and ^{26}Al exposure
240 ages obtained from both sample types on the Hatcher unit, assumed to be pre-LGM in
241 age (Figure 1b). In addition, we sampled the outermost moraine and associated
242 outwash terrace of the younger (est. LGM) Río Blanco unit as a ‘geologic blank’
243 allowing a test of the following fundamental assumptions: (1) terraces stabilized
244 shortly after moraine deposition; (2) nuclide inheritance is low; (3) post-depositional
245 shielding is minimal; and (4) terrace sediment are not mixed post-depositionally. If
246 valid, exposure ages from all samples of the younger Río Blanco unit should be
247 indistinguishable and date the timing of the event.

248

249 For the Hatcher moraines, degradation and erosion is expected to complicate
250 interpretation of boulder exposure ages. To address the relative magnitude of these
251 processes, we sampled moraine cobbles. Because negligible rock surface erosion can
252 be inferred from the preservation of smooth, rounded cobble surfaces, lower nuclide
253 concentrations in cobbles relative to boulders will likely be the result of shielding by
254 the moraine matrix, provided that $^{26}\text{Al}/^{10}\text{Be}$ ratios are not consistent with prolonged
255 burial. Thus moraine cobble nuclide concentrations can help to estimate the amount
256 of degradation. On the Hatcher outwash terrace we additionally sampled a ^{10}Be
257 concentration depth-profile to exploit the depth dependency of cosmogenic nuclide
258 production. These data provide further constraints on the average nuclide inheritance,
259 deposition age and exposure history of the outwash sediment while allowing checks
260 on sediment mixing that could affect exposure ages obtained from individual surface
261 clasts.

262

263 3.1 Sampling

264

265 3.1.1 Sampling criteria and methods

266

267 Moraine boulders were sampled with hammer and chisel following established
268 protocols (e.g., Gosse and Phillips, 2001). We preferentially sampled the top few
269 centimeters of large (> 1 meter) stable boulders (granite) on or near moraine crests
270 showing minimal evidence of surface erosion (Figure 3c). Moraine and outwash
271 cobbles of quartz (5 – 25 cm long axis) were sampled to obtain a sufficient quartz
272 yield and because monomineralic quartz clasts are resistant to weathering. These
273 were collected whole from well-preserved moraine crests (Figure 3c) and from terrace
274 surfaces away from moraines and scarps. The samples were later crushed whole
275 (small cobbles/pebbles) or after cutting to an appropriate thickness, and subsequently
276 sieved to obtain the 250 – 710 μm fraction.

277

278 The depth profile was sampled in a small quarry along Route 40 (Figure 4) at a
279 location where the surrounding surface appeared undisturbed by the excavation. The
280 deposit is composed of cobbles to coarse sands throughout (Figure 3e). Soils are
281 poorly developed in the top 10 – 15 cm (<30% fines at top of profile) and about 40%
282 of the deposit is cemented by pedogenic carbonate at ~30 – 100 cm depth. The bulk
283 density was estimated based on grain size distribution at 2.57 g cm^{-3} with an assumed
284 error of $\pm 0.1 \text{ g cm}^{-3}$ (cf. Hancock et al., 1999). This is based on the observation that
285 75% of the deposit contains grain sizes larger than coarse sands with a clast density of
286 2.7 g cm^{-3} (30% porosity), an interstitial sand density of 2.7 g cm^{-3} (30% porosity) and
287 a pedogenic carbonate density of 2.4 g cm^{-3} occupying 40% of the remaining

288 interstitial space. Eight samples were collected at depths ranging from 10 – 150 cm.
289 Each sample was composed of ten to fifty quartz pebbles (2 – 4 cm) that were
290 amalgamated following Repka et al. (1997). We use the thickness of the largest clast
291 in each sample as measure of the uncertainty of depth (Table 1).

292

293 **3.1.2 Sample location**

294

295 Sample locations are shown in Figures 2 and 4. We sampled the outermost moraine
296 crest and, where possible, from outwash terraces that can be directly mapped to the
297 corresponding dated moraine. Both moraine crests are generally sparsely vegetated
298 with desert pavements (gravels – cobbles) formed at some locations (Figure 3d).
299 Most moraine boulders are ventifacted while rounded moraine cobbles are more often
300 not; neither show rock varnish. The Río Blanco moraines were sampled on the south
301 side of the valley where they are best preserved. The moraines are hummocky but
302 largely continuous with ~20 – 25 meters of relief and slopes of ~20°. The Hatcher
303 moraines are situated 100 m above the Río Blanco outwash and were sampled in more
304 lateral positions on both sides of the valley (over 30 km apart). Moraine relief ranges
305 from 20 – 30 m above the associated outwash terrace to the east (~18° slopes) and
306 from 40 – 50 m above an inter-moraine depression to the west (19° – 25° slopes).

307

308 The Río Blanco and Hatcher outwash terraces occupy ~240 km² and 325 km² in area,
309 respectively. The surfaces dip gently eastward at < 0.5° and converge at the entrance
310 to, and above the Cañadón de Caracoles (Figure 2). Both terraces are composed of
311 gravels and coarse sands with local concentrations of cobbles and pebbles. These
312 small lag deposits are not underlain by fine sediments (i.e., they are not inflationary

313 desert pavements). Vegetation cover is sparse. Shallow surface channels (1 – 3 m)
314 are well-preserved with clear braiding patterns visible; these often grade to recessional
315 moraine positions. Río Blanco outwash was sampled at a location where it could be
316 directly traced to the dated moraine. The Hatcher outwash was sampled at two
317 locations on the northern terrace (Figure 4). Here, three minor (1 – 3m) terrace levels
318 grade to a common base level and can be traced to Hatcher recessional ice limits
319 further west. The first sample site (S1) can be directly mapped to the dated moraine.
320 The second site (S2), which is also the location of the depth-profile, occupies a similar
321 stratigraphic position but is located ~8 km from the dated moraine.

322

323 **3.2 Depth-profile exposure model optimization**

324

325 The depth-profile allows defining the age and erosion rate of the terrace surface and
326 testing of several underlying assumptions. In-situ ^{10}Be production in the upper few
327 meters of the Earth's surface is dominated by high-energy neutron spallation reactions
328 that decrease exponentially with attenuation of the secondary cosmic ray flux at depth.
329 Assuming the Hatcher terrace material was deposited in a single event and remained
330 stable with a single continuous erosion rate, we would expect to observe a smooth
331 exponential decrease of nuclide concentration within the profile that can be described
332 by an appropriately parameterized model. The expected ^{10}Be concentration at depth
333 (z) can be modeled for any given terrace age (t), erosion rate (ε_{terr}), overburden
334 density (ρ) and inherited nuclide concentration (N_{inh}) using the following analytical
335 approximation for production at depth in a steadily eroding deposit (after Granger and
336 Smith, 2000):

337

$$\begin{aligned}
N &= N_{inh} e^{-t\lambda} \\
&+ \left[P_n e^{-\rho z / \Lambda} / (\lambda + \rho \varepsilon_{terr} / \Lambda) \right] \left[1 - e^{-t(\lambda + \rho \varepsilon_{terr} / \Lambda)} \right] \\
&+ \left[P_{\mu 1} e^{-\rho z / L_1} / (\lambda + \rho \varepsilon_{terr} / L_1) \right] \left[1 - e^{-t(\lambda + \rho \varepsilon_{terr} / L_1)} \right] \\
&+ \left[P_{\mu 2} e^{-\rho z / L_2} / (\lambda + \rho \varepsilon_{terr} / L_2) \right] \left[1 - e^{-t(\lambda + \rho \varepsilon_{terr} / L_2)} \right] \\
&+ \left[P_{\mu}^{fast} e^{-\rho z / L_3} / (\lambda + \rho \varepsilon_{terr} / L_3) \right] \left[1 - e^{-t(\lambda + \rho \varepsilon_{terr} / L_3)} \right]
\end{aligned} \tag{1}$$

339

340 where N is the ^{10}Be concentration, N_{inh} is the inherited ^{10}Be concentration, λ is the
341 ^{10}Be radioactive decay constant ($5.1 \times 10^{-7} \text{ a}^{-1}$) (Nishiizumi et al., 2007), P_n , $P_{\mu 1}$, $P_{\mu 2}$ and
342 P_{μ}^{fast} are production rates due to neutron spallation, negative muon capture (μ_1 , μ_2) and
343 fast muon reactions, while Λ (160 g cm^{-2}), L_1 (738.6 g cm^{-2}), L_2 (2688 g cm^{-2}) and L_3
344 (4360 g cm^{-2}) are the respective attenuations lengths provided by Granger and Smith
345 (2000). Production rates for each reaction were calculated as a fraction of the total
346 surface production rate with $f_n = 0.9724$, $f_{\mu 1} = 0.0186$, $f_{\mu 2} = 0.004$ and $f_{\mu}^{fast} = 0.005$
347 integrated over the sample thickness (P_n only; cf. Vermeesch, 2007). The time-
348 averaged surface production rate value is $8.22 \text{ atoms } ^{10}\text{Be g}^{-1} \text{ a}^{-1}$ (Dunai, 2001) (see
349 supplementary material).

350

351 Assuming the terrace deposit experienced a simple exposure history at a constant
352 erosion rate, there should be only one combination of exposure age, terrace erosion
353 rate, overburden density and nuclide inheritance that best fits all the measured data
354 points in the profile. A forward model can be used to obtain the parameters that
355 minimize the difference between the predicted and observed nuclide concentrations.
356 In this study, we use the sum of chi-squared ($\Sigma \chi^2$) for the exposure model
357 optimization. Because the bulk density was estimated in the field (Section 3.1.1), we
358 solve for the exposure duration (t), erosion rate (ε_{terr}) and nuclide inheritance (N_{inh})

359 that best fit the measured profile data and their associated analytical uncertainties (σ_i),
360 such that:

361

$$362 \quad \sum \chi^2 \equiv \sum_{i=1}^N \left(\frac{y_i - y(t, \varepsilon_{terr}, N_{inh})}{\sigma_i} \right)^2 \quad (2)$$

363

364 where y_i is the measured ^{10}Be concentration at a particular sample depth and
365 $y(t, \varepsilon_{terr}, N_{inh})$ is the modeled ^{10}Be concentration at that depth for any given $(t, \varepsilon_{terr}, N_{inh})$
366 solution. The analytical uncertainties (σ_i) include both sample and blank $^{10}\text{Be}/^9\text{Be}$
367 uncertainties and a 2% carrier addition/sample mass uncertainty. For a quantitative
368 assessment of the model's ability to describe the measured data, we assess the
369 'goodness of fit' to the data using the reduced chi-squared (χ_r^2) value. The χ_r^2 is the
370 sum of chi-squared divided by the degrees of freedom, and this value should approach
371 1 if the fitting function describes the data well (cf. Bevington and Robinson, 2003, p.
372 194). The exposure model therefore allows a best estimate of the terrace age, erosion
373 rate and average nuclide inheritance by the sum of chi-squared, and allows us to
374 quantify (χ_r^2) how well the data fit the underlying model.

375

376 **3.3 Exposure age calculations**

377

378 The ^{10}Be and ^{26}Al exposure ages were calculated with the CRONUS-Earth exposure
379 age calculator (version 2.2 ;Balco et al., 2008)² which implements the revised ^{10}Be
380 standardization and half-life (1.36 Ma) of Nishiizumi et al. (2007). Exposure ages are
381 reported based on the Dunai (2001) scaling model; these differ by up to ~5%

² (http://hess.ess.washington.edu/math/index_dev.html)

382 depending on the choice of alternative scaling model. The calculator uses sample
383 thickness (Table 2) and density (assumed 2.7 g cm^3) to standardize nuclide
384 concentrations to the rock surface. Topographic shielding was measured but is
385 negligible (scaling factor <0.9998). We apply no correction for snow or vegetation
386 shielding. No erosion rate correction is applied to the cobble data, but an erosion rate
387 of 1.4 mm ka^{-1} is used to document this effect on boulder exposure ages; this value
388 was derived by Kaplan et al. (2005) for boulders on the Telken moraines at LBA,
389 60km to the north. Sample elevations were converted to air pressures for input into
390 the calculator; we assumed a standard atmosphere for the elevation-pressure
391 relationship. The local sea-level (SL) pressure and temperature ($1009.3 \text{ hPa}/285\text{K}$)³
392 was used to convert elevations to air pressures for samples of the younger Río Blanco
393 unit. We used a lower SL pressure for the conversion of the older Hatcher samples as
394 described below.

395

396 The time-averaged ^{10}Be and ^{26}Al production rates near Lago Pueyrredón have been
397 estimated to be 5% and 11% higher than for standard atmospheric conditions by two
398 independent studies that infer a low pressure anomaly during glacial times (cf. Ackert
399 et al., 2003; Staiger et al., 2007). Following Staiger et al. (2007), we increase ^{10}Be
400 and ^{26}Al production rates by $\sim 5\%$ for samples on the older Hatcher unit (for
401 discussion see supplementary material). We note that, however, that the conclusions
402 of this paper are not sensitive to the choice of correction used. The 5% higher
403 production rate was implemented within the exposure age calculator by artificially
404 lowering the air pressure at the sampled locations, thereby increasing the production
405 rates. Specifically, we lowered the SL pressure that was used in the conversion of

³ NCEP-NCAR reanalysis; www.cdc.noaa.gov/ncep_reanalysis/

406 sample elevations to sample air pressures; the present day SL pressure (1009.3 hPa)
407 was lowered to 1002.3 hPa. The lower SL pressure reduces the calculated sample air
408 pressures, and thereby increases the time-averaged production rate derived through
409 the calculator by approximately 5% when compared against the value obtained from a
410 calculation based on the present day SL pressure.

411

412 **4. RESULTS**

413

414 The analytical results are presented in Tables 1 and 2 and Figures 4 – 7. Samples
415 were prepared at the University of Edinburgh’s Cosmogenic Isotope Laboratory.
416 Information on the chemical procedure is provided in the supplementary material.
417 The AMS measurements were conducted at the AMS-facility at SUERC.
418 Measurements are normalized to the NIST SRM-4325 Be standard material with a
419 revised (Nishiizumi et al., 2007) nominal $^{10}\text{Be}/^9\text{Be}$ ratio of 2.79×10^{-11} , and the
420 Purdue Z92-0222 Al standard material with a nominal $^{27}\text{Al}/^{26}\text{Al}$ ratio of 4.11×10^{-11}
421 which agrees with the Al standard material of Nishiizumi et al. (2004). The $^{26}\text{Al}/^{10}\text{Be}$
422 production rate ratio is 6.69. Samples are corrected for the number of ^{10}Be and ^{26}Al
423 atoms in their associated blanks. Blanks ($n = 8$) were spiked with $250 \mu\text{g } ^9\text{Be}$ carrier
424 and $1.5 \text{ mg } ^{27}\text{Al}$ carrier. Samples were spiked with $250 \mu\text{g } ^9\text{Be}$ carrier and up to 1.5
425 $\text{mg } ^{27}\text{Al}$ carrier (the latter value varied depending on the native Al-content of the
426 sample). For each batch of 7 samples one blank was processed. The corresponding
427 combined process and carrier blanks range between $115,000 \pm 18,000$ atoms ^{10}Be and
428 $290,000 \pm 40,000$ atoms ^{10}Be ($< 3\%$ of total ^{10}Be atoms in sample; $0.9 - 1.7 \times 10^{-14}$
429 [$^{10}\text{Be}/^9\text{Be}$]); and between $61,000 \pm 12,000$ atoms ^{26}Al and $190,000 \pm 57,000$ atoms
430 ^{26}Al ($< 1\%$ of total ^{26}Al atoms in sample; $2.6 - 3.8 \times 10^{-15}$ [$^{27}\text{Al}/^{26}\text{Al}$]). Sample and

431 blank $^{10}\text{Be}/^9\text{Be}$ and $^{27}\text{Al}/^{26}\text{Al}$ analytical uncertainties and a 2% carrier addition
432 uncertainty and 5% stable ^{27}Al measurement (ICP-OES) uncertainty are propagated
433 into the 1σ analytical uncertainty for nuclide concentrations (Tables 1 and 2).
434 Throughout the text, if not stated otherwise, uncertainties are reported as 1σ .
435 Analytical uncertainties are reported, except for means where we report the standard
436 deviation of the population.

437

438 **4.1 Río Blanco unit**

439

440 The ^{10}Be boulder exposure ages from the outermost moraine crest range from 25.4 –
441 32.2 ka (no erosion). The oldest boulder (BC07-8) falls outside 2σ analytical
442 uncertainty of the remaining population. Excluding this sample, the range is from 25
443 – 27 ka and the three ages overlap within error. The arithmetic mean age is 26.0 ± 1.0
444 ka, or 26.8 ± 1.0 including a correction for erosion (sect. 3.3). The three outwash
445 cobbles yield ^{10}Be exposure ages of 24.3 ± 0.8 ka, 24.6 ± 0.8 ka and 25.3 ± 0.7 ka and
446 thus are indistinguishable within uncertainties. The mean outwash cobble age ($24.7 \pm$
447 0.5 ka) is indistinguishable from the boulder mean at 2σ . The low sample variability
448 ($\sigma = 0.5$ ka) of outwash cobbles and indistinguishable ages from moraine boulders
449 confirms our initial assumptions (1-4; see section 3.0).

450

451 **4.2 Hatcher unit**

452

453 **4.2.1 Moraine samples**

454

455 The four moraine boulder samples yield a wide range of ^{10}Be exposure ages from
456 107.4 – 190 ka with a mean of 149.3 ± 37.6 ka (w/erosion; Figure 5). The high
457 standard deviation highlights the significant variability often observed in ‘old’
458 moraine boulder ages. The age range normalized to the oldest boulder (0.38) is
459 typical for moraines (Putkonen and Swanson, 2003). The oldest boulder age (BC07-
460 3) assuming no erosion is 152.8 ± 4.4 ka and corresponds to the tallest boulder
461 sampled on the Hatcher moraines (2m; Figure 3c). The $^{26}\text{Al}/^{10}\text{Be}$ ratios are consistent
462 with relatively simple exposure histories without prolonged burial.

463

464 The moraine cobble ^{10}Be exposure ages range from 41.7 – 57.9 ka with a mean of
465 48.3 ± 6.3 ka (Table 2, Figure 5). The young ages are not thought to be caused by
466 post-depositional burial and re-exposure based on our assessment of the geomorphic
467 environment (Section 2.2). In addition, the $^{26}\text{Al}/^{10}\text{Be}$ ratios are also consistent with a
468 simple exposure history without prolonged burial. Based on this, we infer that low
469 nuclide concentrations (i.e., young exposure ages) are the result of moraine
470 degradation, which appears to be similar at both sample localities > 30 km apart.

471

472 **4.2.2 ^{10}Be concentration depth-profile**

473

474 The depth-profile data is presented in Table 1 and Figures 6 and 7. Figure 7 shows
475 that the ^{10}Be concentration decreases exponentially with depth; consistent with post-
476 deposition production in a stable terrace and no mixing of sediment. We modeled the
477 expected ^{10}Be concentration at depth (see section 3.2) for a range of exposure times (t
478 = 0 – 500 ka; 200 a resolution), terrace erosion rates ($\varepsilon = 0 – 3$ mm ka^{-1} ; 0.01 mm ka^{-1}
479 resolution) and inherited ^{10}Be concentrations (0 – 180,000 atoms g^{-1} ; 30000 atoms g^{-1}

480 resolution) to obtain the parameters that yielded the minimum value for the sum of
481 chi-squared ($\Sigma\chi^2_{min}$). The terrace erosion rate was restricted to positive values in this
482 exercise because pedologic evidence (Section 3.1.1) and geomorphic observations
483 indicate deflation (as opposed to inflation) of the terrace surface (Section 3.1.2). The
484 best fit ($\Sigma\chi^2_{min}$) occurs with 233.8 ka exposure, a terrace erosion rate of 0 mm ka⁻¹ and
485 no inherited nuclides (Figure 6). Figure 6a is the $\log_{10}\Sigma\chi^2$ solution surface for the case
486 of no inheritance. The 1 σ and 2 σ analytical uncertainty contours illustrate the strong
487 correlation between the uncertainties in exposure age and erosion rate. The contours
488 include a wide range of potential exposure age/erosion rate solutions.

489

490 The reduced chi-squared χ_r^2 value of 0.97 indicates the model fit is as good as can be
491 expected given the measurement uncertainties. Figure 7a provides the predicted
492 concentrations, based on the parameters obtained from the best-fit exposure model,
493 against the measured data points. The deepest sample is critical to defining the best-
494 fit parameters. Several exposure age/erosion rate solutions can fit the near surface
495 data well, but are less able to fit the deepest sample. Figure 7b gives the predicted
496 nuclide concentration for two exposure age/erosion rate scenarios that fit most
497 measured data points well, except the deepest samples. This illustrates the importance
498 of deep samples to obtain robust age constraints from depth, and the value of forward
499 modeling to obtain the best fitting parameters.

500

501 **4.2.3 Outwash cobbles**

502

503 Cobbles from the associated outwash terrace yield ¹⁰Be exposure ages that are
504 consistently older than boulder ages, ranging from 193.6 – 265.1 ka. Exposure ages

505 from sample sites S1 and S2 are indistinguishable (Table 2, Figures 4-5). The high
506 variability in exposure ages likely stems from geomorphic processes as opposed to
507 variable inherited nuclides. While the depth profile indicates that the terrace sediment
508 has remained stable below 10 cm, all surface cobbles have similar or higher nuclide
509 concentrations than the concentration at 10 cm in the profile. Thus a combination of
510 near surface turbation (e.g., cryoturbation) above 10 cm and terrace erosion by
511 deflation can explain the observed age range. The geologic evidence supports
512 deflation of the terrace surface (Section 3.1.2), causing previously buried cobbles to
513 become exposed in the process (Figure 7c). The scenario is consistent with an
514 observation that the youngest samples at S2 fully retained their fluvial shape, while
515 the oldest cobbles revealed significant ventifaction (Figure 3f, 3g). With no lithologic
516 difference between cobbles, we infer that ventifaction of surface cobbles indicates a
517 longer surface residence time. The two oldest surface cobbles yield an arithmetic
518 mean age of 260.6 ± 6.5 ka (1σ external ± 34 ka; Figure 5). The old ages are unlikely
519 to be the result of re-working of older sediment based on our assessment of nuclide
520 inheritance (Section 5.1) and also because alluvial fans composed of older (Caracoles)
521 sediment are clearly defined and over 5 km from the sampled location (Figure 4). The
522 $^{26}\text{Al}/^{10}\text{Be}$ ratios are consistent with a relatively simple exposure history without
523 prolonged burial.

524

525 **5. DISCUSSION**

526

527 **5.1 Nuclide inheritance**

528

529 We assess nuclide inheritance based on the ^{10}Be concentration depth-profile of pebble
530 clasts, which averages inheritance over 10 to 50 individual pebble clasts per sample at
531 each of the eight sample depths. These data indicate that the average inherited nuclide
532 component in the Hatcher outwash terrace is negligible (Figure 6b). This is in
533 agreement with the low variability of ages found in outwash cobbles from the younger
534 Río Blanco unit ($\sigma = 0.5$ ka), which suggests that the variability of inherited nuclides
535 is low (i.e., within analytical uncertainties), and by inference inheritance (if
536 inheritance would be large, its variability would be large). Thus we conclude that
537 nuclide inheritance is negligible in outwash deposits of the Río Blanco and Hatcher
538 units, and probably throughout the Lago Pueyrredón valley.

539

540 **5.2 Age of the Hatcher Unit**

541

542 The Hatcher moraines and associated outwash terraces were deposited roughly
543 coincidentally, yet exposure ages differ by over 200 ka depending on the sample and
544 nature of the sample location. Because nuclide inheritance is demonstrably low and
545 most geologic processes act to reduce cosmogenic nuclide inventories (Phillips et al.,
546 1990), the oldest ages are considered the best estimate for the deposition age of the
547 unit. The oldest surface cobbles are likely closest to the deposition age at 260.6 ± 6.5
548 ka, analogous to the oldest boulder ages on a moraine (cf. Zreda and Phillips, 1995).
549 This age is ~ 25 ka older than that indicated by the depth-profile $\Sigma\chi^2_{min}$ best-fit at 233.8
550 ka, but is indistinguishable at 1σ (Figure 6a). The statistical best-fit ($\Sigma\chi^2_{min}$) occurs
551 with a terrace erosion rate of 0 mm ka^{-1} . The geologic evidence, however, suggests
552 minor terrace deflation (Section 3.1.2). Changes in bulk density occurring temporally
553 (e.g., with soil and pedogenic carbonate formation) may have influenced the $\Sigma\chi^2_{min}$ fit,

554 but the effect cannot be accurately accounted for and is expected to be small relative
555 to age uncertainty. A terrace age of 260.6 ka corresponds with an inferred terrace
556 erosion rate of ca. 0.53 mm ka⁻¹ based on the depth-profile ($\chi_r^2 = 1.12$; Figures 6a,7c).
557 This suggests ~14 cm of terrace deflation over the exposure duration, with survival of
558 the oldest clasts likely due to their resistant lithology. This amount of surface
559 lowering is consistent with minor terrace deflation inferred at the sampled sites and
560 with preservation of shallow surface channels with clear braiding patterns (~50cm
561 relief). The ²⁶Al/¹⁰Be ratios of surface cobbles and the depth-profile data are
562 consistent with a single stage exposure history. Based on current knowledge of ¹⁰Be
563 production rates and the assumptions made in this paper, we estimate the age of the
564 Hatcher unit to be 260.6 ± 6.5 ka (1σ external ± 34 ka; ε_{terr} = 0.53 mm ka⁻¹).

565

566 Of the five scaling schemes implemented in the CRONUS-Earth exposure age
567 calculator, the time-dependent Lal (1991)/Stone (2000) scaling factors yield the
568 youngest exposure ages by ~5%. Using these scaling factors reduces the interpreted
569 minimum age to 248 ± 24 ka (1σ external). Within uncertainty this overlaps with the
570 age of substage 7d (~ 225 - 220 ka, Martinson et al., 1987). However, substage 7d is
571 short-lived relative to both MIS 6 and 8. The Hatcher unit is older than MIS 6, and its
572 size and preservation suggests it was more extensive than MIS 6. Thus we consider it
573 unlikely that the Hatcher moraines are age-equivalent to the short-lived 7d substage,
574 and consider it more likely that they are coeval with the more pronounced global
575 cooling during MIS 8, as indicated by our estimated exposure age.

576

577 **5.2.1 Discordant ages**

578

579 The above results indicate that in certain environments the outwash terrace is a better
580 target for exposure dating old glacial events than the associated moraine. Outwash
581 samples yield consistently older exposure ages than those from the moraines (Figure
582 5). This result was expected based on the favorable environmental conditions and
583 local geomorphology (Section 1.3 – 2). However, the significant disparity in ages
584 between moraine boulders and outwash cobbles was not predicted. While large
585 scatter is expected of old moraine boulders, the oldest age was thought to date closely
586 moraine deposition. In this case, that age was more than 100 ka too young. Putkonen
587 and Swanson (2003) recommend sampling at least 6 – 7 boulders from old and tall
588 moraines to obtain a boulder age at $\geq 90\%$ of the moraine age (95% confidence).
589 Therefore we cannot rule-out under-sampling as a cause of the discrepancy.
590 However, well-preserved boulders were rare.

591

592 The $^{26}\text{Al}/^{10}\text{Be}$ ratios provide no evidence to explain the young boulder ages. Boulder
593 erosion rate uncertainty could explain the wide scatter and young ages, but the
594 moraine cobble data (where negligible erosion is implicit) indicate that exhumation
595 (moraine degradation) is likely the primary control. The moraine cobble with the
596 highest ^{10}Be concentration (5.26×10^5 atoms g^{-1}) is used to infer minimum moraine
597 degradation rates using model scenarios (Equation 1) that assume a deposition age of
598 260 ka and a till density of 2.2 g cm^{-3} . The minimum amount occurs with instant
599 degradation of ~ 101 cm at the time of sampling. By comparison, the concentration
600 can be achieved with a constant degradation rate of 12 mm ka^{-1} , equating to ~ 3.1
601 meters of surface lowering. The tallest boulder (2.0 m) has an exposure age within
602 30% of the age of the outwash terrace, which may indicate a relatively small amount

603 of original cover. Concluding, we infer that boulder exhumation is the primary cause
604 of the young and scattering boulder exposure ages.

605

606 However, additional complexity may have been introduced by episodic boulder
607 erosion. If significant aeolian erosion occurs when outwash plains are active (Section
608 2.2), then aeolian erosion episodes probably occurred during MIS 6 (ca. 150 ka) and
609 during deposition of the Río Blanco outwash at ~25 ka. Because the erosion rate
610 applied is a long-term average, a relatively recent pulse of boulder erosion may yield
611 exposure ages that are too young (e.g., Small et al., 1997). However, aeolian erosion
612 is normally restricted to less than 50 cm above the soil surface (Bagnold, 1941), thus
613 the taller boulders may not have experienced it in the geologically recent past.

614

615 Moraine cobbles are rarely ventifacted, suggesting exhumation occurred after any
616 recent (aeolian) erosion episode. For the sake of argument, if we assume soil
617 degradation at a constant rate, the derived rate (12 mm ka^{-1}) is nearly double the
618 maximum rate estimated for the older and more subdued Telken moraines at LBA (ca.
619 7 mm ka^{-1} ; Ackert and Mukhopadhyay, 2005). By comparison, the Hatcher moraines
620 are relatively sharp crested at the sampled locations (Figure 3c,d). Because
621 environmental conditions are similar, the different rates could be explained by a
622 differing moraine surface morphology. Models predict higher degradation on tall and
623 steeply dipping moraines (Putkonen and O'Neal, 2006; Putkonen and Swanson, 2003).
624 At the sampled location, the ice-contact flank of the moraine was taller (40 – 50 m
625 high) and steeper dipping ($19^\circ - 25^\circ$) than both the down-ice flank, and more subdued
626 terminal locations. It is possible this 'lateral moraine' morphology at the sampled
627 locations could result in locally high degradation. If so, the large discrepancy in

628 boulder and outwash ages could be due in part to our choice of sample location,
629 despite seemingly good preservation.
630
631 Regardless of the cause, our data highlight the significant challenges of exposure
632 dating old glacial deposits using moraine boulders. Despite probable exhumation of
633 all boulder samples and complexity introduced by boulder erosion, the data yield a
634 typical spread of ages with the oldest boulder age (no erosion) and the average age
635 (w/erosion) indistinguishable. This together with an observation of moraine ridges as
636 old as 1.1 Ma still clearly preserved (Figure 2) would suggest that moraine
637 degradation rates are generally low in this environment. Given only this information,
638 it would be reasonable to assume the exposure ages from boulder samples (~150 ka)
639 dated closely moraine deposition. However, this interpretation would be erroneous by
640 over 100 ka. It is worth noting that small moraine cobbles are highly sensitive to
641 moraine degradation in this environment, these samples yield exposure ages that
642 underestimate the deposition age by over 200 ka. These results highlight the
643 challenge of exposure dating old moraines and suggest a cautious approach to
644 interpreting such data.

645

646 **5.3 Correlation to LBA record**

647

648 The new cosmogenic exposure ages allow comparison to the record at LBA. We re-
649 calculate the ^{10}Be boulder exposure ages published by Kaplan et al. (2004; 2005) and
650 Douglass et al. (2006) for both the Fenix V and Moreno II moraines in order to
651 compare directly the data presented in this study and the assumptions therein. The
652 Río Blanco – Fenix correlation is valid based on LGM ages of 26.8 ± 1.0 ka and 24.5

653 ± 1.3 ka for the Río Blanco and Fenix moraines, respectively. The Hatcher – Moreno
654 correlation is less convincing. On Moreno II, the oldest ^{10}Be boulder exposure age
655 (no erosion) of 169.4 ka and mean age (w/erosion) of 168.8 ka is indistinguishable
656 from the Hatcher boulders. If the supposed correlation is valid, then the Moreno
657 moraines were also deposited at ~ 260 ka, and the young boulder exposure ages on the
658 Moreno moraines are analogous to those of the Hatcher moraines. Alternatively, the
659 correlation may not be valid and these are indeed two different glacial events
660 preserved separately in each valley.

661

662 The available evidence supports the latter interpretation. First, the lowest ^{10}Be
663 concentration of 5 moraine cobbles on Moreno I was found to be $\sim 7.30 \times 10^5$ atoms g^{-1}
664 (Table 3). With steady degradation, this concentration can be achieved with rates of
665 6.1 and 7.6 mm ka^{-1} for a surface ~ 170 ka (oldest boulder age) and ~ 260 ka (Hatcher
666 age), respectively. These rates are consistent with the maximum rate estimated for the
667 Telken moraines in this valley (Ackert and Mukhopadhyay, 2005), and equate to
668 roughly 105 – 200 cm of moraine surface lowering. Thus degradation rates are
669 apparently lower for the Moreno moraines and boulders may have been continuously
670 exposed. Second, 6-7 boulders (cf. Putkonen and Swanson, 2003) between 5 – 200
671 cm height were measured from the Moreno I-II moraines; these were age consistent
672 (Kaplan et al., 2005). Third, $^{230}\text{Th}/\text{U}$ dating of soil carbonate formed in outwash
673 gravels associated with the Moreno II moraines suggest onset of calcic pedogenesis at
674 170 ± 8.3 ka (Phillips et al., 2006). $^{230}\text{Th}/\text{U}$ data from the younger Fenix moraines
675 indicates a brief interval (< 3 ka) between surface stabilization and the onset of calcic
676 pedogenesis under glacial conditions. The re-calculated ^{10}Be boulder exposure ages
677 are consistent with this new data. Therefore, based on the available evidence, the best

678 estimate for the age of the Moreno I-II moraines is before ~170 ka, or MIS 6, and thus
679 the correlation to the Hatcher moraines appears invalid on this basis.

680

681 **6. CONCLUSIONS**

682

- 683 • We demonstrate that outwash terrace sediments are better targets than
684 associated moraine boulders for exposure dating ‘old’ (i.e., pre-LGM) glacial
685 deposits in the Lago Pueyrredón valley, central Patagonia. A comparatively
686 small number of outwash samples provide more consistently accurate results.
- 687 • We find that exposure ages from moraine boulders underestimate the
688 deposition age by ~100 ka, and exposure ages from moraine cobbles
689 underestimate the deposition age by over 200 ka. We infer that exhumation as
690 a consequence of moraine degradation is the primary cause of the age
691 discrepancy between the moraine and outwash samples.
- 692 • A forward model inversion of a ^{10}Be depth-profile in the outwash terrace
693 sediment, using the sum of chi-squared, is used to define the exposure age,
694 erosion rate and inherited ^{10}Be concentration. This model, in conjunction with
695 geologic observations and exposure ages from surface cobbles, indicates a
696 terrace age of ca. 260 ka, a low terrace erosion rate of ca. 0.5 mm ka^{-1} , and no
697 inherited nuclides.
- 698 • The result indicates that a major advance of a Patagonian ice sheet occurred at
699 ~260 ka (MIS 8) and deposited the Hatcher moraines at Lago Pueyrredón.
700 This finding differs from findings at Lago Buenos Aires, where the Moreno I-
701 II moraines, which occupy a similar stratigraphic position relative to the LGM

702 deposits, are dated to MIS 6 (Kaplan et al., 2005). This documents the value
703 of more than one site in a region for reconstructing glacial chronologies.

- 704 • The local LGM maximum occurred at ~27 – 25 ka and is represented by the
705 Río Blanco moraine system.
- 706 • No deposits relating to MIS 6 or MIS 4 were observed at Lago Pueyrredón.
- 707 • Our ages for the Río Blanco and Hatcher moraines are discrepant with the
708 previously inferred chronology (Wenzens, 2005).

709

710 **ACKNOWLEDGEMENTS**

711

712 We thank C. Risso, P. Alvarez and O. Martínez for logistical support; A-S. Meriaux
713 for fieldwork support; S. Binnie and E. McDougall for assistance with laboratory
714 work and D. Sugden for helpful comments. We thank the UK Natural Environment
715 Research Council, the Royal Geographic Society (with IBG) - Rio Tinto plc award,
716 the Royal Scottish Geographic Society and the Carnegie Trust for the Universities of
717 Scotland for support of this study. We thank the Scottish Universities Environmental
718 Research Centre (S.U.E.R.C.) for sample analysis. We are grateful for the
719 constructive comments of two anonymous reviewers that greatly improved the
720 manuscript. This is L-DEO contribution number #XXXX.

721

722 **Figure 1**

723

- 724 a) Location of study area showing an expanded Patagonian ice sheet and the
725 present day North (NPI) and South (SPI) Patagonian Icefields with

726 glacial/interglacial specific drainage pattern. The Rio Baker presently
727 drains both Lago Buenos Aires (LBA) and Lago Pueyrredón (LP).
728 b) The over-deepened (white=high elevation) LBA and LP outlet valleys with
729 comparison of the broad glacial stratigraphy and mapping of Caldenius
730 (1932). The chronology at LBA is based on cosmogenic exposure ages
731 (^3He , ^{10}Be , ^{26}Al) by Kaplan et al. (2004, 2005) and Douglass et al. (2006)
732 and limiting $^{40}\text{Ar}/^{39}\text{Ar}$ ages by Singer et al. (2004). The naming
733 convention used for glacial units in the LP valley is based on Caldenius
734 (1932).

735

736 **Figure 2**

737

738 DEM (SRTM 90m, artificially illuminated) of the LP valley showing ice limits of the
739 four major glacial units and the exceptional preservation of moraine and outwash
740 terraces. The well-preserved moraines of the Gorra de Poivre ice limit are inferred to
741 be 1.1 Ma. The sampled locations for each sample type in this study are shown along
742 with ^{14}C dates by Wenzens (2005) and Mercer (1982) and magnetic polarity
743 measurements by Sylwan et al. (1991)(see section 2.3).

744

745 **Figure 3**

746

747 a) Granite moraine boulder with flutings demonstrating the erosive power of
748 debris laden wind. Varying degrees of wind erosion is common to
749 moraine boulders and outwash cobbles.

- 750 b) Quartz pebble from the Hatcher outwash terrace (S1) showing rock varnish
751 on ventifacts which suggests aeolian erosion is episodic.
- 752 c) The tallest (2m) and oldest boulder sampled from the sharp-crested
753 Hatcher moraine on the north side of valley.
- 754 d) The Hatcher moraine crest on the south side of the valley, showing a desert
755 pavement of cobble and pebble clasts.
- 756 e) Photo of the depth-profile location with pedogenic carbonate formation
757 below ~30cm depth. The top of the profile was undisturbed and vegetated.
758 The top 10 cm of the profile contains less than ~30% fine material.
- 759 f) The youngest surface cobbles at S2 retained their fluvial shape, indicating
760 relatively recent exhumation.
- 761 g) The oldest surface cobbles at S2 showed significant wind erosion
762 (ventifacted facet at the top right of the cobble) indicating a long surface
763 residence time.

764

765 **Figure 4**

766

767 Geomorphic map of the Hatcher moraines and outwash terraces on the north side of
768 valley (location shown in Figure 2), showing sample locations and exposure ages.

769 Three small (1 – 3m difference in elevation) terrace levels related to recessional
770 moraine limits are clearly distinguished close to their associated moraines, but grade
771 to a common base level further east. Outwash was sampled at two sites (S1 and S2).

772 S1 can be directly mapped to the dated moraine while S2 is located 8 km NE at a
773 point where the small terrace levels coalesce; the exposure ages obtained from

774 samples from S1 and S2 are indistinguishable. The location of outwash fans
775 composed of older “Caracoles” material is shown. DP: depth-profile location.

776

777 **Figure 5**

778

779 ^{10}Be exposure ages obtained from samples of the Río Blanco and Hatcher units at
780 Lago Pueyrredón, 47.5° S, Argentina, compared to the Vostok temperature curve
781 (Petit et al., 1999). Data is ordered by sample type. Cartoon depicts moraine and
782 outwash positions but is not to scale. S1 and S2 refer to sample sites on Hatcher
783 outwash terrace (Figure 4). Exposure ages obtained using the CRONUS-Earth
784 exposure age calculator (<http://hess.ess.washington.edu/math/index.html>) version 2.2
785 (Balco et al., 2008) with a 5% higher production rate for Hatcher samples (Section
786 3.3) and Dunai (2001) scaling factors. Uncertainties are 1σ analytical. Boulder
787 erosion rates from Kaplan et al. (2005). The Río Blanco data show little variability
788 compared to the Hatcher data. The mean of the two oldest outwash terrace cobbles
789 (red-line) is the interpreted age of the glacial advance, moraine boulders under-
790 estimate this age by ~ 100 ka. See Table 2 for full sample details.

791

792 **Figure 6**

793

794 a) Plot of the gridded $\log_{10}(\Sigma\chi^2)$ values for a range of exposure ages and
795 erosion rates for the case of no inherited nuclides; the plot is based on the
796 depth-profile data and exposure model optimization. The sensitivity to
797 inheritance is illustrated in Figure 6b. The best-fit (star) occurs with an
798 exposure age of 233.8 ka, an erosion rate of 0 mm ka^{-1} and no inherited

799 nuclides. Contours are increments of 0.5 from the $\log_{10}(\Sigma\chi^2)$ minimum.
800 The uncertainty contours mark the probability of occurrence ($0.68/1\sigma$,
801 $0.90/2\sigma$) for 5 degrees of freedom. The model fits analytical sources of
802 uncertainty as discussed in the text. The uncertainties of exposure age and
803 erosion rate are strongly correlated. The inferred terrace age, based on the
804 mean exposure age of the oldest surface cobbles (these were not included
805 in the profile optimization), corresponds to a terrace erosion rate of ~ 0.53
806 mm ka^{-1} .

807 b) Plot showing the effect of varying the exposure age, erosion rate and ^{10}Be
808 inheritance on the $\Sigma\chi^2$ minimum value for a range of inheritance values.
809 The maximum inheritance value was obtained from the nuclide
810 concentration of the deepest sample in the profile (Table 1). The $\Sigma\chi^2_{min}$
811 steadily increases as the total inheritance increases; thus the best fit occurs
812 with no inherited nuclides.

813

814 **Figure 7**

815

816 Measured ^{10}Be concentration as a function of depth within the Hatcher outwash
817 terrace. Data points (solid circles) are an amalgamation of pebble clasts following
818 Repka et al. (1997) (Table 1). The (1σ) analytical uncertainties in ^{10}Be concentration
819 were used in the model optimization. The uncertainty with depth is based on the
820 thickness of the largest clast (Table 1).

821 a) Plot of modeled best-fit ($\Sigma\chi^2_{min}$) ^{10}Be concentration based on the exposure
822 model optimization.

862 the French Western Alps from Be-10 dating of alluvial terraces with
863 assessment of inheritance, soil development and wind ablation effects. *Earth*
864 *and Planetary Science Letters* **209**, 197-214.

865 Caldenius, C. R. C. (1932). "Las glaciaciones cuaternarias en la Patagonia y Tierra del
866 Fuego : una investigación regional, estratigráfica y geocronológica : una
867 comparación con la escala geocronológica sueca : with an English summary."
868 [Stockholms högskola], Stockholm.

869 Chadwick, O. A., Hall, R. D., and Phillips, F. M. (1997). Chronology of Pleistocene
870 glacial advances in the central Rocky Mountains. *Geological Society of*
871 *America Bulletin* **109**, 1443-1452.

872 Chorley, R. J., Schumm, S. A., and Sugden, D. E. (1984). "Geomorphology."
873 Methuen, London, New-York.

874 Clapperton, C. M. (1993). "Quaternary Geology and Geomorphology of South
875 America." Elsevier Science Publishers B. V., Amsterdam.

876 Douglass, D. C., Singer, B. S., Kaplan, M. R., Mickelson, D. M., and Caffee, M. W.
877 (2006). Cosmogenic nuclide surface exposure dating of boulders on last-
878 glacial and late-glacial moraines, Lago Buenos Aires, Argentina: Interpretive
879 strategies and paleoclimate implications. *Quaternary Geochronology* **1**, 43-58.

880 Dunai, T. J. (2001). Influence of secular variation of the geomagnetic field on
881 production rates of in situ produced cosmogenic nuclides. *Earth and Planetary*
882 *Science Letters* **193**, 197-212.

883 Flint, R. F., and Fidalgo, F. (1964). Glacial Geology Of The East Flank Of The
884 Argentine Andes Between Latitude 39-Degrees-10's And Latitude 41-
885 Degrees-20's. *Geological Society of America Bulletin* **75**, 335.

886 Gillespie, A. R., and Bierman, P. R. (1995). Precision of terrestrial exposure ages and
887 erosion rates estimated from analysis of cosmogenic isotopes produced in situ.
888 *Journal of Geophysical Research-Solid Earth* **100**, 24637-24649.

889 Gosse, J. C., and Phillips, F. M. (2001). Terrestrial in situ cosmogenic nuclides:
890 theory and application. *Quaternary Science Reviews* **20**, 1475-1560.

891 Granger, D. E., and Smith, A. L. (2000). Dating buried sediments using radioactive
892 decay and muogenic production of Al-26 and Be-10. *Nuclear Instruments &*
893 *Methods in Physics Research Section B-Beam Interactions with Materials and*
894 *Atoms* **172**, 822-826.

895 Hallet, B., and Putkonen, J. (1994). Surface Dating Of Dynamic Landforms - Young
896 Boulders On Aging Moraines. *Science* **265**, 937-940.

897 Hancock, G. S., Anderson, R. S., Chadwick, O. A., and Finkel, R. C. (1999). Dating
898 fluvial terraces with Be-10 and Al-26 profiles: application to the Wind River,
899 Wyoming. *Geomorphology* **27**, 41-60.

900 Hulton, N. R. J., Purves, R. S., McCulloch, R. D., Sugden, D. E., and Bentley, M. J.
901 (2002). The Last Glacial Maximum and deglaciation in southern South
902 America. *Quaternary Science Reviews* **21**, 233-241.

903 Inbar, M., Osters, H. A., Parica, C. A., Remesal, M. B., and Salani, F. M. (1995).
904 Environmental Assessment of 1991 Hudson Volcano Eruption Ashfall Effects
905 on Southern Patagonia Region, Argentina. *Environmental Geology* **25**, 119-
906 125.

907 Kaplan, M. R., Ackert, R. P., Singer, B. S., Douglass, D. C., and Kurz, M. D. (2004).
908 Cosmogenic nuclide chronology of millennial-scale glacial advances during
909 O-isotope stage 2 in Patagonia. *Geological Society of America Bulletin* **116**,
910 308-321.

- 911 Kaplan, M. R., Coronato, A., Hulton, N. R. J., Rabassa, J. O., Kubik, P. W., and
912 Freeman, S. (2007). Cosmogenic nuclide measurements in southernmost
913 South America and implications for landscape change. *Geomorphology* **87**,
914 284-301.
- 915 Kaplan, M. R., Douglass, D. C., Singer, B. S., and Caffee, M. W. (2005). Cosmogenic
916 nuclide chronology of pre-last glacial maximum moraines at Lago Buenos
917 Aires, 46 degrees S, Argentina. *Quaternary Research* **63**, 301-315.
- 918 Kaplan, M. R., Hein, A. S., Hubbard, A., and Lax, S. M. (2009). Can glacial erosion
919 limit the extent of glaciation? *Geomorphology* **103**, 172-179.
- 920 Kaplan, M. R., Singer, B. S., Douglass, D. C., Ackert, R. P., and Caffee, M. W.
921 (2006). Comment on: Cosmogenic nuclide chronology of pre-last glacial
922 maximum moraines at Lago Buenos Aires, 46 degrees S, Argentina
923 (Quaternary Research 63/3, 2005, 301-315) - Reply. *Quaternary Research* **66**,
924 367-369.
- 925 Lal, D. (1991). Cosmic-Ray Labeling Of Erosion Surfaces - Insitu Nuclide
926 Production-Rates And Erosion Models. *Earth And Planetary Science Letters*
927 **104**, 424-439.
- 928 Martinson, D. G., Pisias, N. G., Hays, J. D., Imbrie, J., Moore, T. C., and Shackleton,
929 N. J. (1987). Age Dating and the Orbital Theory of the Ice Ages -
930 Development of a High-Resolution-0 to 300,000-Year Chronostratigraphy.
931 *Quaternary Research* **27**, 1-29.
- 932 Meglioli, A. (1992). "Glacial geology and chronology of southernmost Patagonia and
933 Tierra del Fuego, Argentina and Chile." Lehigh University.
- 934 Mercer, J. H. (1976). Glacial History Of Southernmost South-America. *Quaternary*
935 *Research* **6**, 125-166.
- 936 Mercer, J. H. (1982). Holocene glacier variations in southern South America. *Striae*
937 **18**, 35-40.
- 938 Nishiizumi, K. (2004). Preparation of Al-26 AMS standards. *Nuclear Instruments &*
939 *Methods in Physics Research Section B* **223-24**, 388-392.
- 940 Nishiizumi, K., Imamura, M., Caffee, M. W., Southon, J. R., Finkel, R. C., and
941 McAninch, J. (2007). Absolute calibration of Be-10 AMS standards. *Nuclear*
942 *Instruments & Methods in Physics Research Section B* **258**, 403-413.
- 943 Owen, L. A., Caffee, M. W., Bovard, K. R., Finkel, R. C., and Sharma, M. C. (2006).
944 Terrestrial cosmogenic nuclide surface exposure dating of the oldest glacial
945 successions in the Himalayan orogen: Ladakh Range, northern India.
946 *Geological Society Of America Bulletin* **118**, 383-392.
- 947 Petit, J. R., Jouzel, J., Raynaud, D., Barkov, N. I., Barnola, J. M., Basile, I., Bender,
948 M., Chappellaz, J., Davis, M., Delaygue, G., Delmotte, M., Kotlyakov, V. M.,
949 Legrand, M., Lipenkov, V. Y., Lorius, C., Pepin, L., Ritz, C., Saltzman, E.,
950 and Stievenard, M. (1999). Climate and atmospheric history of the past
951 420,000 years from the Vostok ice core, Antarctica. *Nature* **399**, 429-436.
- 952 Phillips, F. M., Zreda, M. G., Evenson, E. B., Hall, R. D., Chadwick, O. A., and
953 Sharma, P. (1997). Cosmogenic Cl-36 and Be-10 ages of Quaternary glacial
954 and fluvial deposits of the Wind River Range, Wyoming. *Geological Society*
955 *of America Bulletin* **109**, 1453-1463.
- 956 Phillips, F. M., Zreda, M. G., Smith, S. S., Elmore, D., Kubik, P. W., and Sharma, P.
957 (1990). Cosmogenic Chlorine-36 Chronology for Glacial Deposits at Bloody
958 Canyon, Eastern Sierra-Nevada. *Science* **248**, 1529-1532.
- 959 Phillips, R. J., Sharp, W. D., Singer, B. S., and Douglass, D. C. (2006). Utilising U-
960 series disequilibria of calcic soils to constrain the surface age of Quaternary

- 961 deposits: A comparison with ^{10}Be , ^{26}Al age data from Patagonian glacial
962 moraines. *Geochimica et Cosmochimica Acta* **70**, A491.
- 963 Putkonen, J., Connolly, J., and Orloff, T. (2008). Landscape evolution degrades the
964 geologic signature of past glaciations. *Geomorphology* **97**, 208-217.
- 965 Putkonen, J., and O'Neal, M. (2006). Degradation of unconsolidated Quaternary
966 landforms in the western North America. *Geomorphology* **75**, 408-419.
- 967 Putkonen, J., and Swanson, T. (2003). Accuracy of cosmogenic ages for moraines.
968 *Quaternary Research* **59**, 255-261.
- 969 Rabassa, J., and Clapperton, C. M. (1990). Quaternary Glaciations Of The Southern
970 Andes. *Quaternary Science Reviews* **9**, 153-174.
- 971 Rabassa, J., Coronato, A., Bujalesky, G., Salemme, M., Roig, C., Meglioli, A.,
972 Heusser, C., Gordillo, S., Roig, F., Borromei, A., and Quattrocchio, M. (2000).
973 Quaternary of Tierra del Fuego, Southernmost South America: an updated
974 review. *Quaternary International* **68**, 217-240.
- 975 Repka, J. L., Anderson, R. S., and Finkel, R. C. (1997). Cosmogenic dating of fluvial
976 terraces, Fremont River, Utah. *Earth and Planetary Science Letters* **152**, 59-
977 73.
- 978 Schäfer, J. M., Oberholzer, P., Zhao, Z., Ivy-Ochs, S., Wieler, R., Baur, H., Kubik, P.
979 W., and Schluchter, C. (2008). Cosmogenic beryllium-10 and neon-21 dating
980 of late Pleistocene glaciations in Nyalam, monsoonal Himalayas. *Quaternary
981 Science Reviews* **27**, 295-311.
- 982 Schildgen, T., Dethier, D. P., Bierman, P., and Caffee, M. (2002). Al-26 and Be-10
983 dating of late Pleistocene and Holocene fill terraces: A record of fluvial
984 deposition and incision, Colorado Front Range. *Earth Surface Processes and
985 Landforms* **27**, 773-787.
- 986 Shanahan, T. M., and Zreda, M. (2000). Chronology of quaternary glaciations in East
987 Africa. *Earth and Planetary Science Letters* **177**, 23-42.
- 988 Singer, B. S., Ackert, R. P., and Guillou, H. (2004). Ar-40/Ar-19 and K-Ar
989 chronology of Pleistocene glaciations in Patagonia. *Geological Society of
990 America Bulletin* **116**, 434-450.
- 991 Singer, B. S., and Pringle, M. S. (1996). Age and duration of the Matuyama-Brunhes
992 geomagnetic polarity reversal from Ar-40/Ar-39 incremental heating analyses
993 of lavas. *Earth and Planetary Science Letters* **139**, 47-61.
- 994 Small, E. E., Anderson, R. S., Repka, J. L., and Finkel, R. (1997). Erosion rates of
995 alpine bedrock summit surfaces deduced from in situ Be-10 and Al-26. *Earth
996 and Planetary Science Letters* **150**, 413-425.
- 997 Staiger, J., Gosse, J., Toracinta, R., Oglesby, B., Fastook, J., and Johnson, J. V.
998 (2007). Atmospheric scaling of cosmogenic nuclide production: Climate
999 effect. *Journal of Geophysical Research-Solid Earth* **112**.
- 1000 Stone, J. O. (2000). Air pressure and cosmogenic isotope production. *Journal Of
1001 Geophysical Research-Solid Earth* **105**, 23753-23759.
- 1002 Suárez, M., and De La Cruz, R. (2001). Jurassic to miocene K-Ar dates from eastern
1003 central Patagonian Cordillera plutons, Chile (45 degrees-48 degrees S).
1004 *Geological Magazine* **138**, 53-66.
- 1005 Sugden, D. E., McCulloch, R. D., Bory, A., and Hein, A. S. (2009). Influence of
1006 Patagonian glaciers on Antarctic dust deposition during the last glacial period.
1007 *Nature Geoscience* **d.o.i. (10.1038/NGEO474)**.
- 1008 Sylwan, C., Beraza, L., and Caselli, A. (1991). Magnetoestratigrafia de la secuencia
1009 morenica en el valle del Lago Pueyrredon, provincia de Santa Cruz.
1010 *Asociacion Geologica Argentina, Rev.* **XLVI**, 235-238.

- 1011 Ton-That, T., Singer, B., Mörner, N., and Rabassa, J. (1999). Datación de lavas
1012 basálticas por $^{40}\text{Ar}/^{39}\text{Ar}$ geología glacial de la region del lago Buenos Aires,
1013 provincia de Santa Cruz, Argentina. *Revisita de la Asociación Geológica*
1014 *Argentina* **54**, 333-352.
- 1015 Vermeesch, P. (2007). CosmoCalc: An Excel add-in for cosmogenic nuclide
1016 calculations. *Geochemistry Geophysics Geosystems* **8**.
- 1017 Wenzens, G. (2005). Glacier advances east of the Southern Andes between the Last
1018 Glacial Maximum and 5,000 BP compared with lake terraces of the endorrheic
1019 Lago Cardiel (49 degrees S, Patagonia, Argentina). *Zeitschrift Für*
1020 *Geomorphologie* **49**, 433-454.
- 1021 Wenzens, G. (2006). Comment on: Cosmogenic nuclide chronology of pre-last glacial
1022 maximum moraines at Lago Buenos Aires, 46 degrees S, Argentina
1023 (Quaternary Research 63/3, 2005, 301-315). *Quaternary Research* **66**, 364-
1024 366.
- 1025 Zentmire, K. N., Gosse, J., Baker, C., McDonald, E., and Wells, S. (1999). The
1026 problem of inheritance when dating alluvial fans and terraces with TCN:
1027 Insight from the Matanuska Glacier. *GSA Abstracts and Programs* **31**.
- 1028 Zreda, M. G., and Phillips, F. M. (1995). Insights into alpine moraine development
1029 from cosmogenic Cl-36 buildup dating. *Geomorphology* **14**, 149-156.
- 1030 Zreda, M. G., Phillips, F. M., and Elmore, D. (1994). Cosmogenic Cl-36
1031 Accumulation in Unstable Landforms .2. Simulations and Measurements on
1032 Eroding Moraines. *Water Resources Research* **30**, 3127-3136.
- 1033
1034

Supplementary material for on-line publication only

[Click here to download Supplementary material for on-line publication only: Hein_supplement.doc](#)

Table 1: ¹⁰Be data for depth-profile in Hatcher outwash terrace.

Sample ID – AMS ID	Latitude	Longitude	Altitude	Depth	# clasts	Thickness ^a	Quartz mass	¹⁰ Be measured ^b (10 ⁶ atom g ⁻¹) (±1σ)
	(dd)	(dd)	(m asl)	(cm)		(cm)	(g)	
<i>depth-profile (S2)</i>								
BC07-48a – b2068	-47.26627	-70.96320	583	10	41	3	21.65	1.508 ± 0.047
BC07-48b – b2067				20	14	3.5	27.42	1.242 ± 0.039
BC07-48c – b2066				30	10	3.5	39.06	1.153 ± 0.033
BC07-48d – b2063				40	18	4	46.18	0.948 ± 0.029
BC07-48e – b2062				50	37	4	58.19	0.802 ± 0.023
BC07-48f – b2061				75	19	4	63.82	0.563 ± 0.018
BC07-48g – b2048				100	49	3.5	59.44	0.381 ± 0.010
BC07-48h – b2060				150	44	3	61.54	0.184 ± 0.006

a. Thickness of largest clast included in profile; this is used as a measure of depth uncertainty in the profile. b.

Nuclide concentrations are normalized to revised ¹⁰Be standards and half-life (1.36 Ma) of Nishiizumi et al. (2007) and include propagated AMS sample/lab-blank uncertainty and 2% carrier mass uncertainty. Clast density 2.7 g cm⁻³.

³. Topographic shielding at the profile site is negligible. All AMS measurements made at S.U.E.R.C.

Table 2

[Click here to download Table: Hein_Table2.doc](#)

Table 2: ^{10}Be and ^{26}Al data for Río Blanco and Hatcher moraines and outwash terraces.

Sample I.D.	Latitude	Longitude	Altitude	Boulder height	Thickness	Quartz mass	Isotope	Nuclide concentration ^a	$^{26}\text{Al}/^{10}\text{Be}^b$	Age 1 ^{c,d} (10^3 yrs)		Age 2 ^{c,d,e} (10^3 yrs)		
										$\varepsilon = 0$	$\pm 1\sigma$ (int)	$\pm 1\sigma$ (ext)	$\varepsilon = 1.4 \text{ mm ka}^{-1}$	$\pm 1\sigma$ (int)
	(dd)	(dd)	(m asl)	(cm)	(cm)	(g)	AMS ID ^a	(10^6 atom g^{-1})						
Río Blanco^d														
<i>moraine boulder</i>														
BC07-7	-47.5186	-71.2361	564	225	2.5	20.9284	$^{10}\text{Be} - \text{b2050}$	0.200 ± 0.007	-	27.1 ± 0.9	3.3	28.0 ± 0.9	3.6	
BC07-8	-47.5564	-71.2629	587	190	1.5	27.7948	$^{10}\text{Be} - \text{b2043}$	0.245 ± 0.008	-	32.2 ± 1.0	3.9	33.4 ± 1.0	4.3	
BC07-12	-47.5840	-71.3548	665	310	1.5	24.1815	$^{10}\text{Be} - \text{b2036}$	0.207 ± 0.007	-	25.4 ± 0.8	3.1	26.2 ± 0.8	3.3	
BC07-43	-47.5079	-71.2451	581	80	1.5	25.7394	$^{10}\text{Be} - \text{b2055}$	0.193 ± 0.006	-	25.5 ± 0.8	3.1	26.2 ± 0.9	3.3	
<i>outwash terrace</i>														
BC06-32	-47.48563	-71.21694	564	-	3.5	24.1803	$^{10}\text{Be} - \text{b2074}$	0.178 ± 0.006	-	24.3 ± 0.8	3.0	-	-	
BC06-34	-47.48602	-71.21705	563	-	4	30.9418	$^{10}\text{Be} - \text{b2075}$	0.185 ± 0.006	-	25.3 ± 0.7	3.1	-	-	
BC06-35	-47.48587	-71.21661	564	-	4	24.7066	$^{10}\text{Be} - \text{b2078}$	0.180 ± 0.006	-	24.6 ± 0.8	3.0	-	-	
Hatcher^d														
<i>moraine boulder</i>														
BC07-1	-47.2946	-71.0865	680	95	2	19.6454	$^{10}\text{Be} - \text{b2049}$	1.188 ± 0.030	-	139.9 ± 3.6	17.4	170.1 ± 5.3	26.3	
BC07-3	-47.2987	-71.0579	673	200	1.5	18.6180	$^{10}\text{Be} - \text{b1767}$	1.290 ± 0.037	7.24 ± 0.48	152.8 ± 4.4	19.2	189.6 ± 6.8	30.5	
							$^{26}\text{Al} - \text{a641}$	9.545 ± 0.554		155.2 ± 10.6	24.9	226.6 ± 18.3	44.4	
BC07-4	-47.2988	-71.0576	678	100	2	20.4468	$^{10}\text{Be} - \text{b2038}$	0.952 ± 0.030	6.46 ± 0.41	111.7 ± 3.5	14.0	129.4 ± 4.7	19.1	
							$^{26}\text{Al} - \text{a647}$	6.154 ± 0.333		109.0 ± 6.0	14.9	126.0 ± 8.1	20.3	
BC07-5	-47.5408	-71.1509	783	135	2	20.0563	$^{10}\text{Be} - \text{b2039}$	0.889 ± 0.028	6.52 ± 0.41	95.0 ± 2.9	11.8	107.2 ± 3.7	15.2	
							$^{26}\text{Al} - \text{a649}$	5.798 ± 0.319		93.3 ± 5.2	12.7	105.2 ± 6.6	16.3	
<i>moraine cobble</i>														
BC06-98	-47.30247	-71.04547	653	-	5	19.6917	$^{10}\text{Be} - \text{b2087}$	0.394 ± 0.013	-	47.7 ± 1.5	5.9	-	-	
BC06-99	-47.30246	-71.04553	652	-	3	21.2545	$^{10}\text{Be} - \text{b2080}$	0.420 ± 0.012	-	50.1 ± 1.4	6.1	-	-	
BC06-37	-47.53	-71.14309	762	-	3.5	15.0548	$^{10}\text{Be} - \text{b1206}$	0.412 ± 0.020	6.54 ± 0.49	44.0 ± 2.1	5.6	-	-	
							$^{26}\text{Al} - \text{a487}$	2.691 ± 0.157		42.8 ± 2.5	5.7	-	-	
BC06-42	-47.53	-71.14294	763	-	4	15.0285	$^{10}\text{Be} - \text{b1207}$	0.526 ± 0.022	5.88 ± 0.41	57.9 ± 2.3	7.3	-	-	
							$^{26}\text{Al} - \text{a488}$	3.091 ± 0.171		50.5 ± 2.8	6.7	-	-	
BC06-43	-47.53	-71.14309	762	-	4	15.5849	$^{10}\text{Be} - \text{b1208}$	0.383 ± 0.014	6.75 ± 0.45	41.7 ± 1.5	5.2	-	-	
							$^{26}\text{Al} - \text{a489}$	2.587 ± 0.143		41.9 ± 2.3	5.5	-	-	
<i>Outwash terrace cobble</i>														
S1	BC06-103	-47.2998	-71.0362	620	-	2.5	19.2727	$^{10}\text{Be} - \text{b2892}$	1.610 ± 0.043	-	203.7 ± 5.5	25.8	-	-
	BC06-104	-47.2998	-71.0362	622	-	2	25.1177	$^{10}\text{Be} - \text{b2893}$	1.832 ± 0.052	-	232.2 ± 6.7	29.8	-	-
	BC06-106	-47.2998	-71.0363	622	-	3	20.9424	$^{10}\text{Be} - \text{b2896}$	1.530 ± 0.039	-	193.6 ± 5.0	24.4	-	-
S2	BC07-50	-47.2661	-70.9641	582	-	4	17.4325	$^{10}\text{Be} - \text{b1772}$	1.970 ± 0.061	6.35 ± 0.41	265.1 ± 8.4	34.5	-	-
							$^{26}\text{Al} - \text{a642}$	12.51 ± 0.710		263.1 ± 16	39.1	-	-	
	BC07-51	-47.2661	-70.9642	582	-	2	19.7668	$^{10}\text{Be} - \text{b2056}$	1.567 ± 0.043	6.62 ± 0.41	204.0 ± 5.6	26.0	-	-
							$^{26}\text{Al} - \text{a657}$	10.37 ± 0.57		209.0 ± 12	30.1	-	-	
	BC07-52	-47.2661	-70.9642	582	-	3.5	11.185	$^{10}\text{Be} - \text{b2037}$	1.592 ± 0.046	-	210.3 ± 6.2	26.8	-	-
	BC07-53	-47.2661	-70.9642	583	-	2.5	20.107	$^{10}\text{Be} - \text{b2057}$	1.932 ± 0.050	6.65 ± 0.46	256.0 ± 6.8	32.9	-	-
							$^{26}\text{Al} - \text{a658}$	12.84 ± 0.82		266.9 ± 19	40.8	-	-	

Samples processed at the University of Edinburgh's Cosmogenic Isotope Laboratory following procedures adapted from the methods of Bierman et al. (2002) and Kohl and Nishiizumi (1992), for details see supplementary material. Shielding is negligible for all samples (shielding factor < 0.9998); rock density 2.7 g cm^{-3} . All AMS measurements made at S.U.E.R.C. normalised to NIST SRM-4325 Be standard material with a revised (Nishiizumi et al., 2007) nominal $^{10}\text{Be}/^9\text{Be}$ ratio (2.79×10^{-11}) and half-life (1.36 Ma), and the Purdue Z92-0222 Al standard material with a nominal $^{27}\text{Al}/^{26}\text{Al}$ ratio of 4.11×10^{-11} that agrees with Al standard material of Nishiizumi et al. (2004). Nuclide concentrations include propagated AMS sample/lab-blank uncertainty, 2% carrier mass uncertainty (Be) and 5% stable ^{27}Al measurement (ICP-OES) uncertainty. b. Surface production ratio begins at 6.69. c. Exposure ages calculated using the CRONUS-Earth web based calculator

version 2.2 (Balco et al., 2008) and Dunai (2001) scaling factors. d. Production rate increased by 5% for Hatcher data only by reducing sample air pressure (SL pressure reduced to 1002.3 hPa). e. Erosion rate from Kaplan et al.(2005) at LBA. (int) = internal (analytical) uncertainties; (ext) = propagated external uncertainties (Balco et al., 2008).

Table 3[Click here to download Table: Hein_Table3.doc](#)

Table 3: ¹⁰Be data for moraine cobbles on the Moreno I moraine at LBA

Sample ID	Latitude	Longitude	Altitude	Thickness	Quartz mass	¹⁰ Be measured ^a
	(dd)	(dd)	(m asl)	(cm)	(g)	(10 ⁵ atom g ⁻¹)
						(±1σ)
LBA06-1	-46.5645	-70.8851	504	3	14.65	7.30 ± 0.24
LBA06-3	-46.5647	-70.8851	504	3.5	11.69	8.38 ± 0.29
LBA06-5	-46.5649	-70.8850	503	3	11.78	6.74 ± 0.25
LBA06-6	-46.5649	-70.8850	503	4	17.01	7.41 ± 0.39
LBA06-7	-46.5649	-70.8850	504	3	15.70	8.56 ± 0.27

a. All AMS measurements made at S.U.E.R.C. normalised to NIST SRM-4325 Be standard material with a revised (Nishiizumi et al., 2007) nominal ¹⁰Be/⁹Be ratio (2.79 x 10⁻¹¹) and half-life (1.36 Ma). Nuclide concentrations include propagated AMS sample/lab-blank uncertainty and 2% carrier mass uncertainty. Shielding is negligible for all samples (shielding factor <0.9998); rock density 2.7 g cm⁻³.

Figure 1 - color on web only
[Click here to download high resolution image](#)

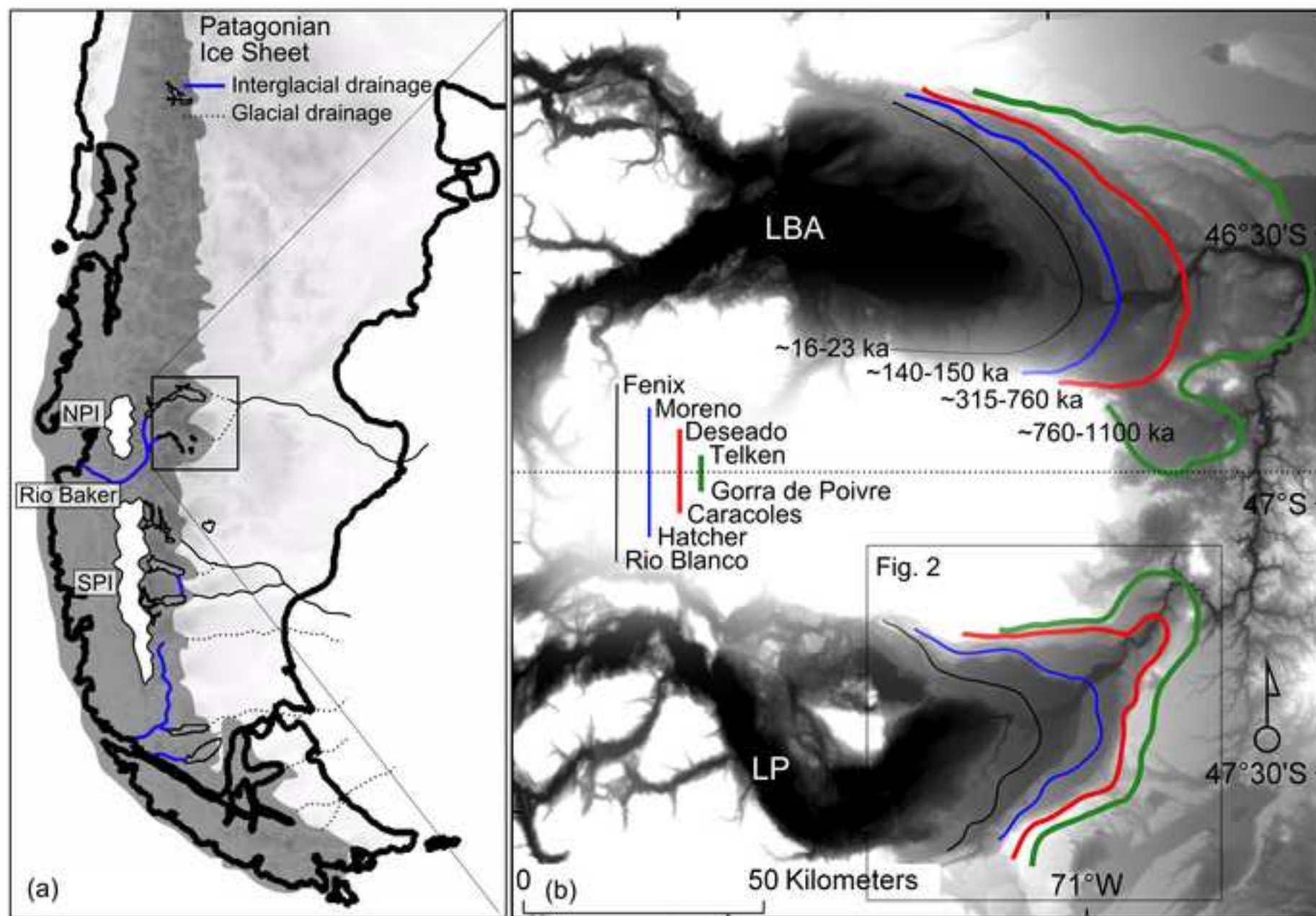
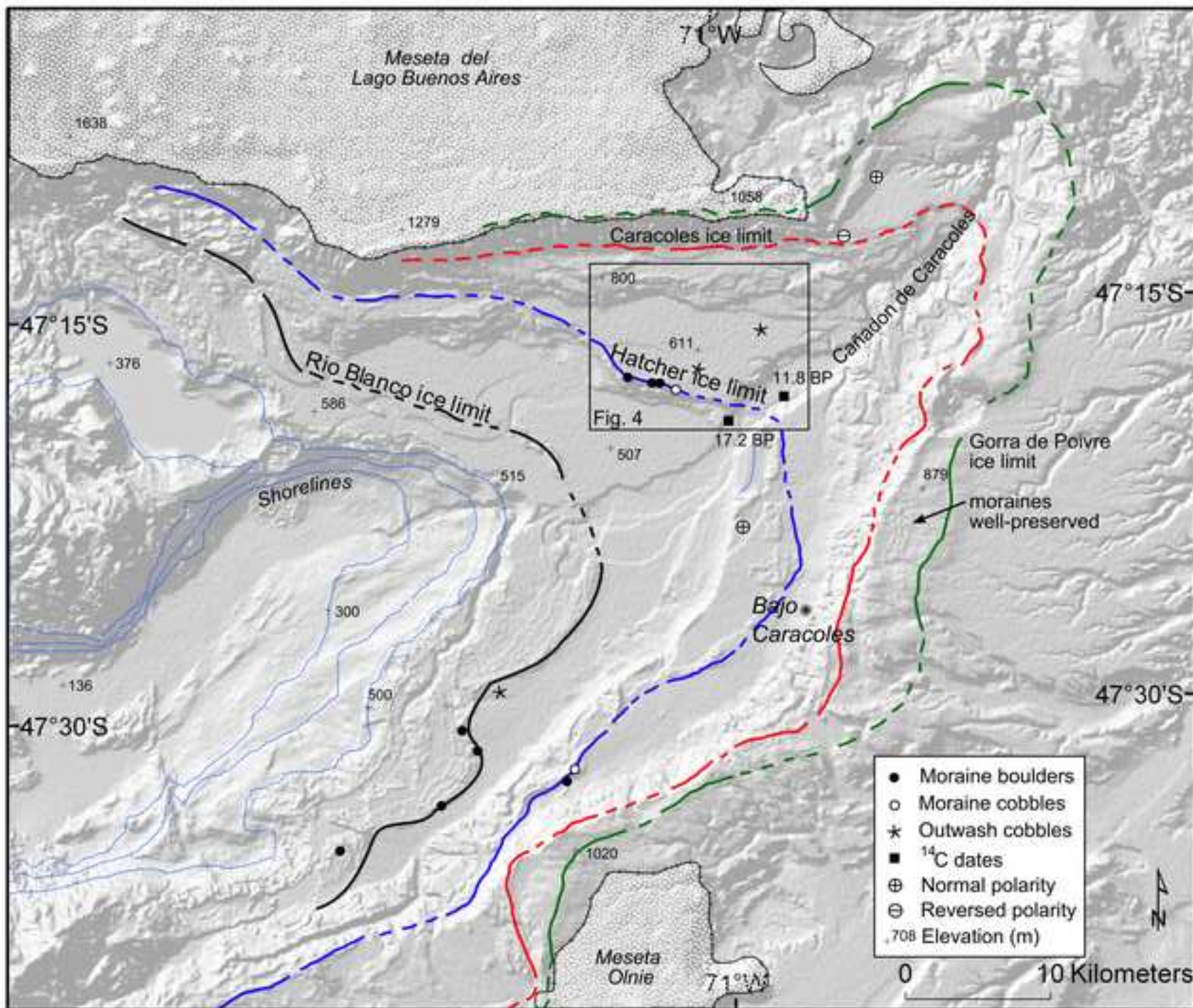


Figure 2 - color on web only
[Click here to download high resolution image](#)



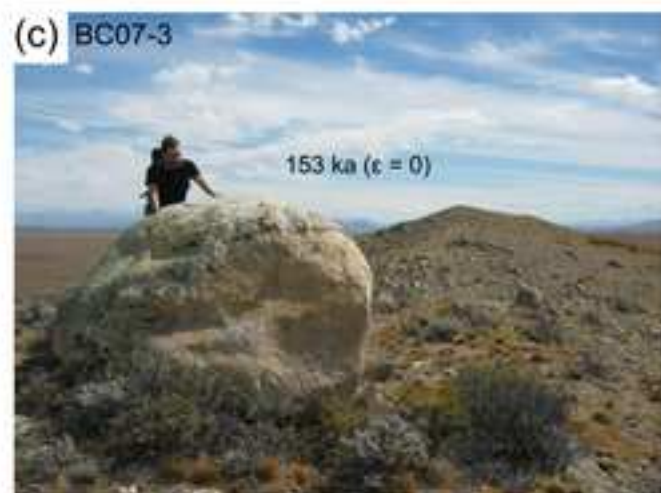


Figure 4
[Click here to download high resolution image](#)

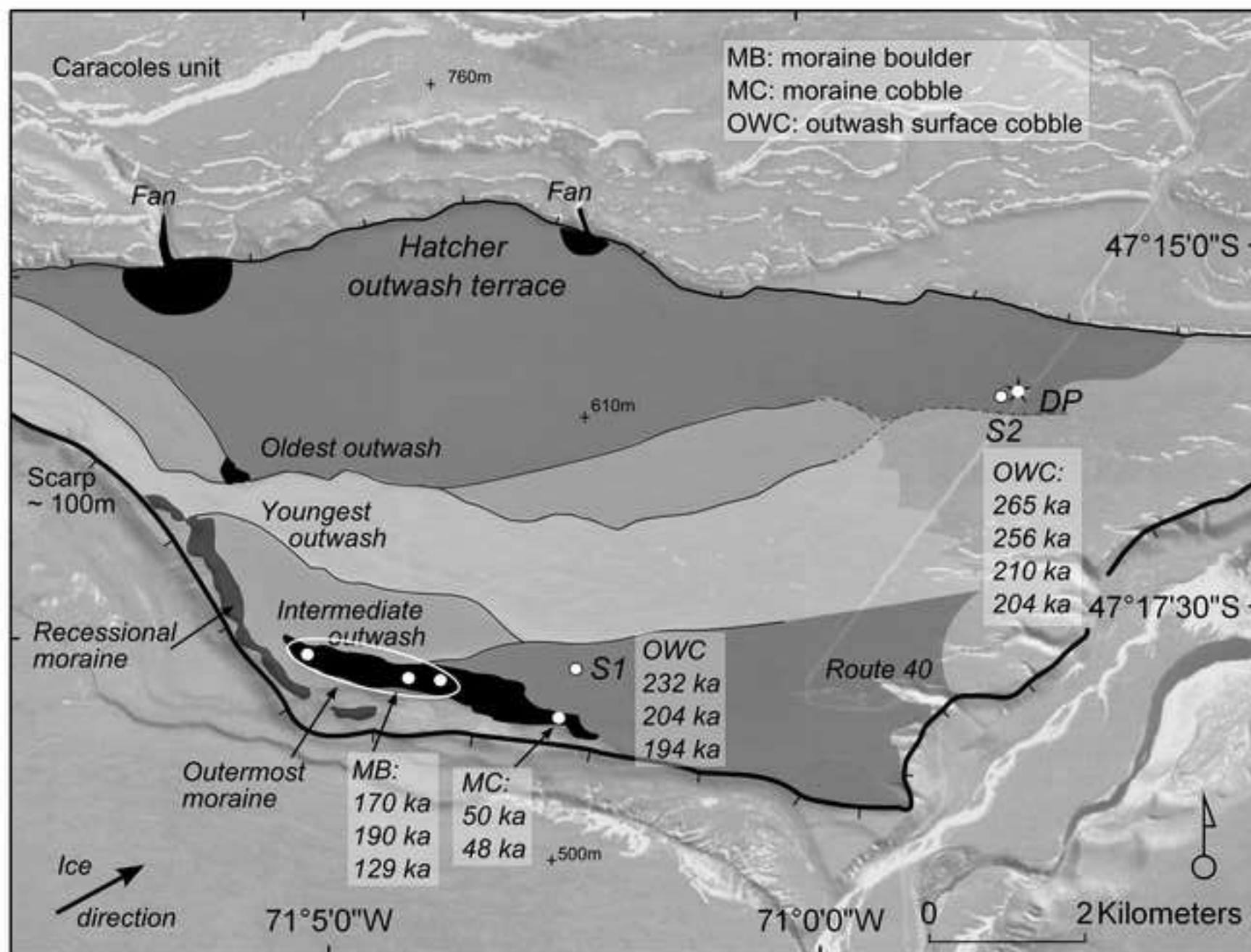


Figure 5 - color on web only
[Click here to download high resolution image](#)

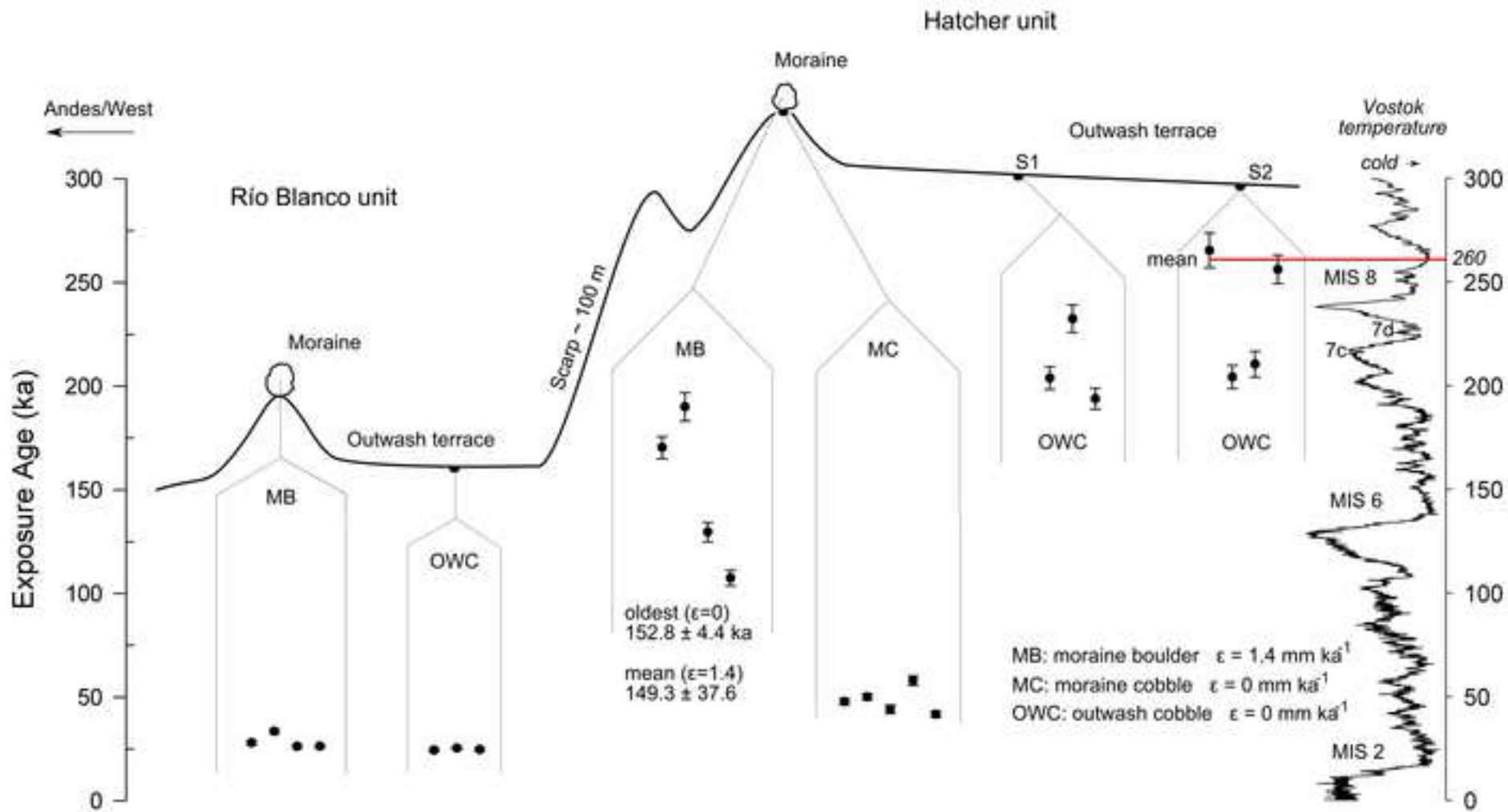


Figure 6a - color on web only
[Click here to download high resolution image](#)

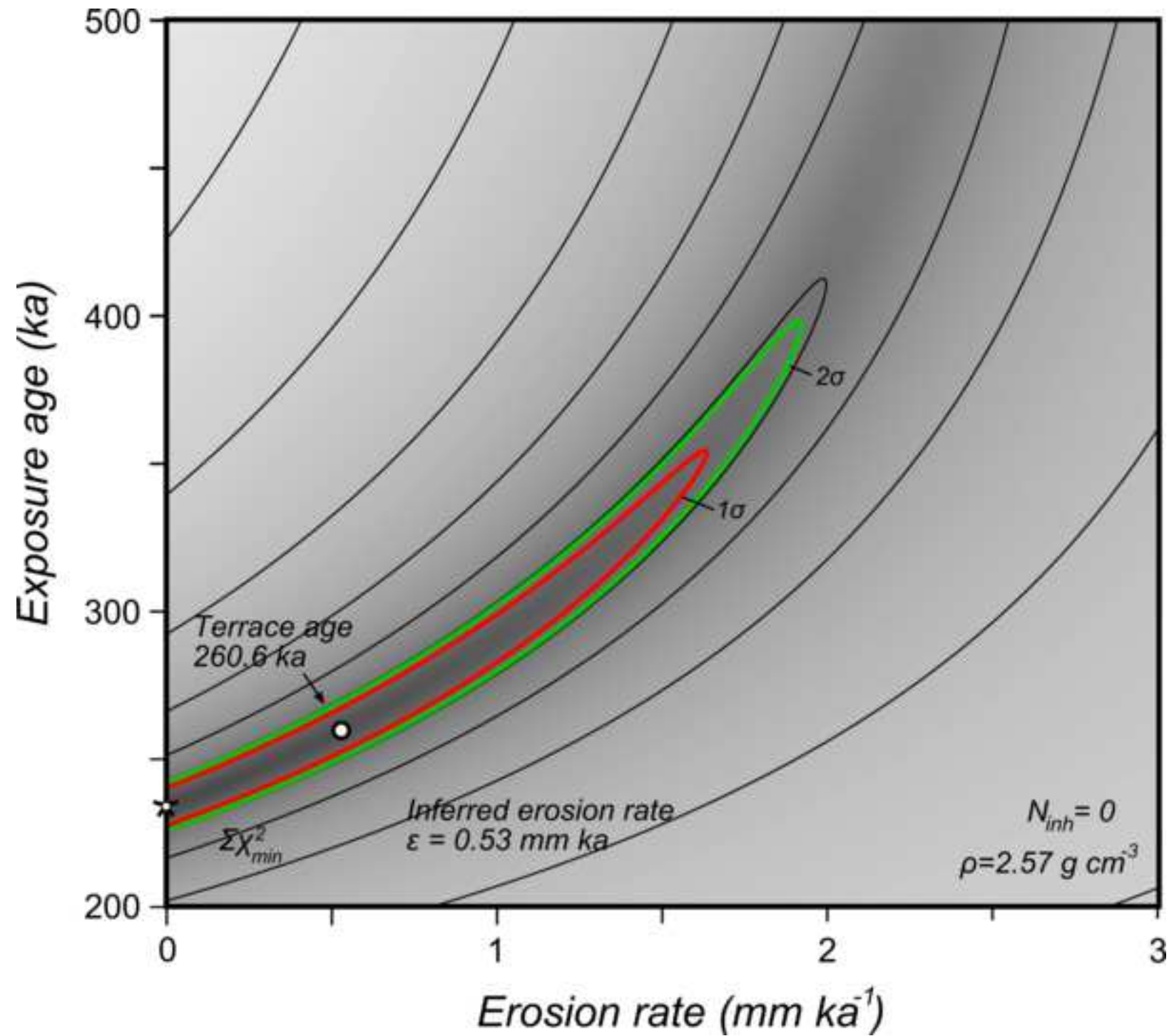


Figure 6b
[Click here to download high resolution image](#)

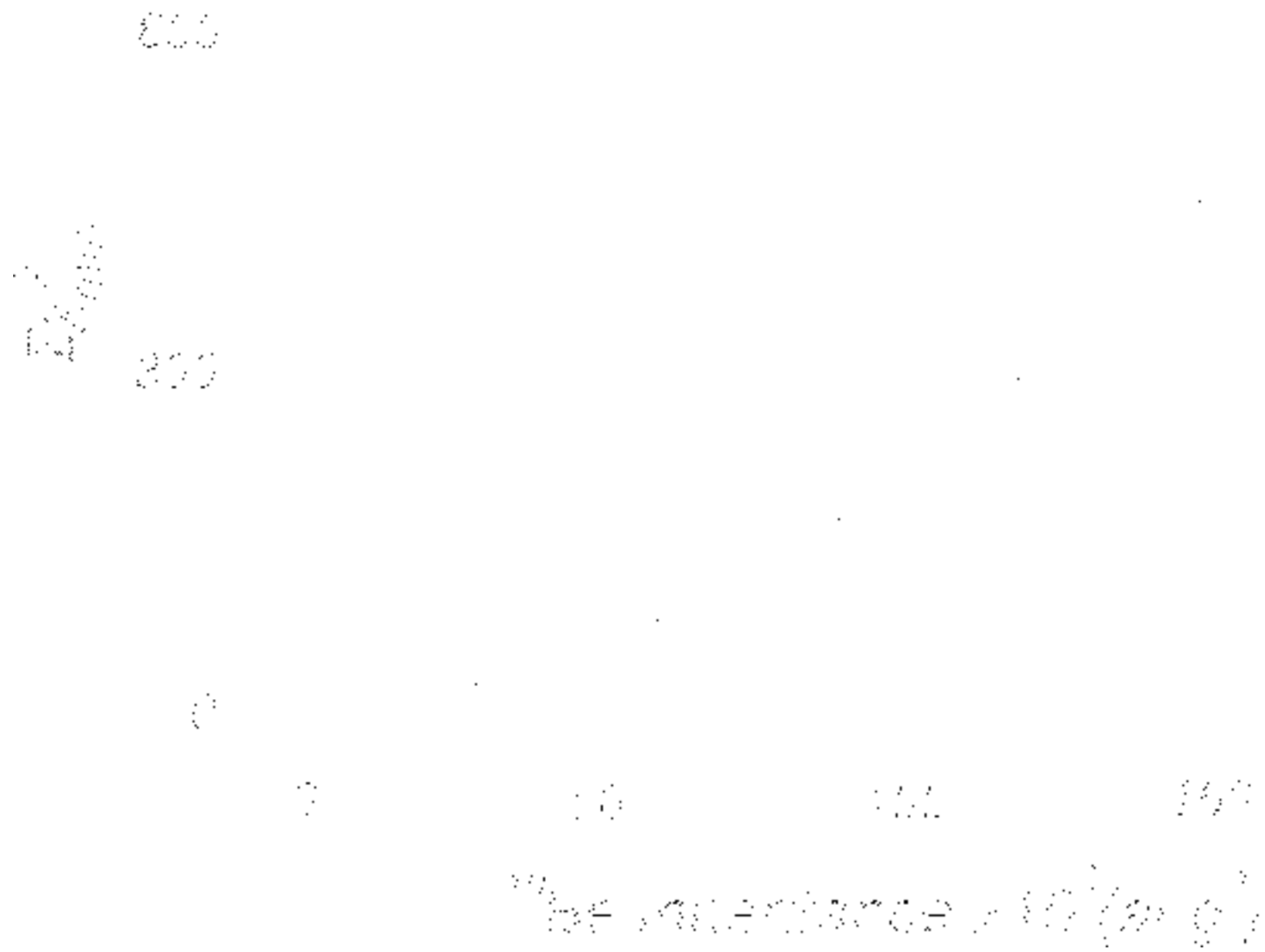


Figure 7a - color on web only
[Click here to download high resolution image](#)

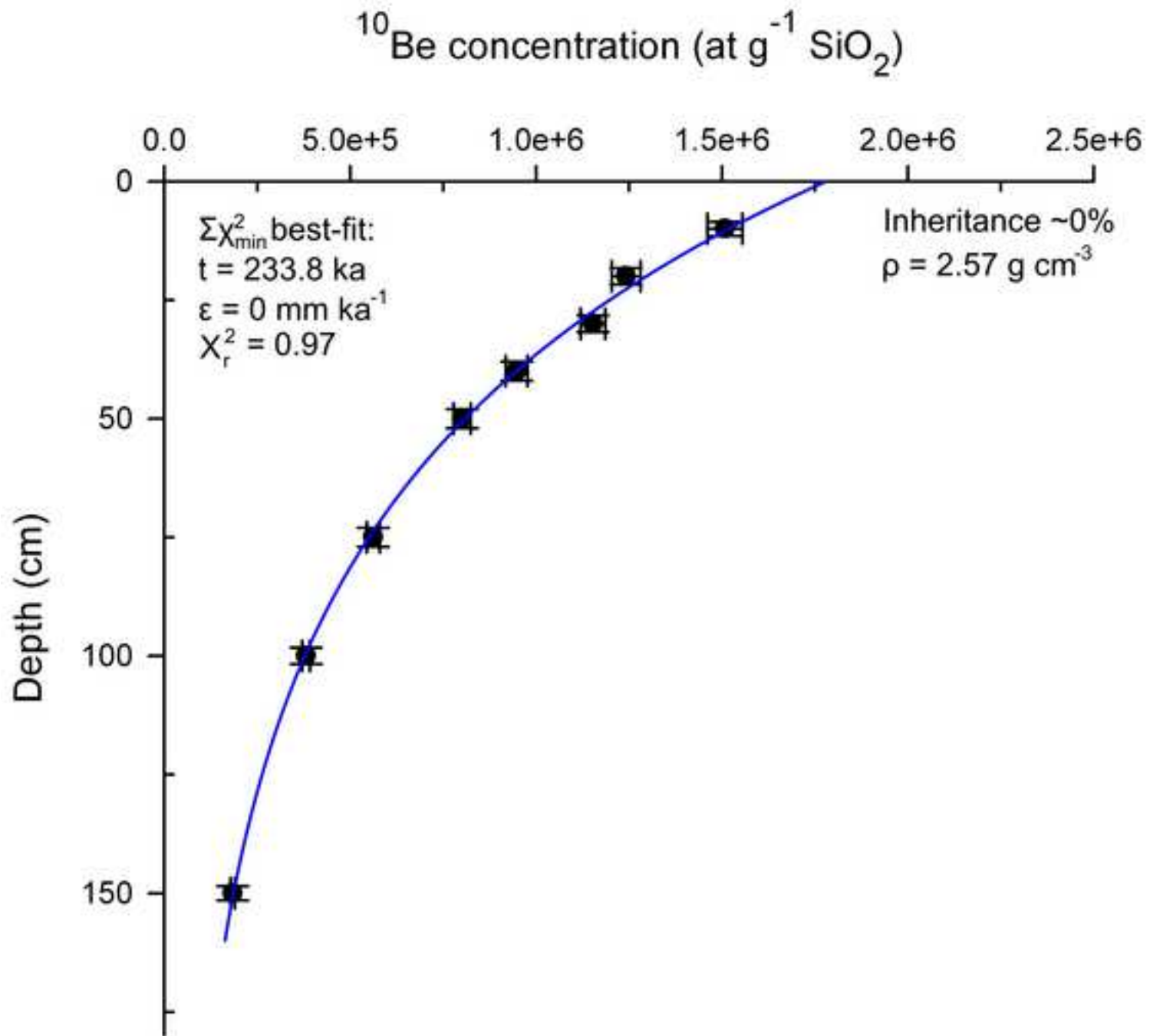


Figure 7b - color on web only
[Click here to download high resolution image](#)

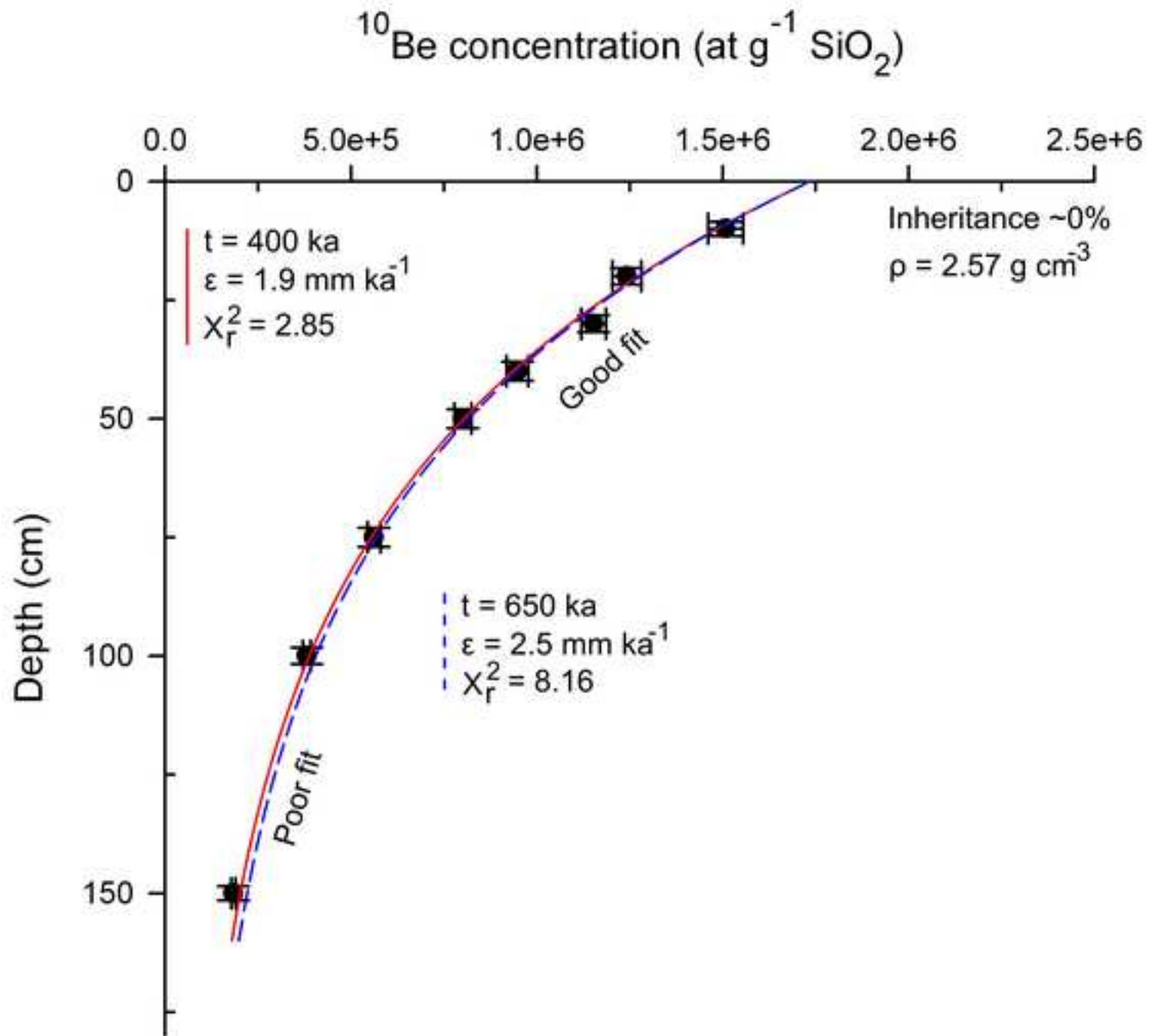


Figure 7c - color on web only
[Click here to download high resolution image](#)

